An Assessment of the Thermal Effects on Striped Bass Larvae Entrained in the Heated Discharge of the Indian Point Generating Facilities Units 2&3

H.H. Carter
R.E. Wilson
G.E. Carroll

SPECIAL REPORT 24

REFERENCE 79-7

MARINE SCIENCES RESEARCH CENTER
STATE UNIVERSITY OF NEW YORK
STONY BROOK, NEW YORK 11794

AN ASSESSMENT OF THE THERMAL EFFECTS ON STRIPED BASS LARVAE ENTRAINED IN THE HEATED DISCHARGE OF THE INDIAN POINT GENERATING FACILITIES UNITS 2&3

H.H. Carter
R.E. Wilson
G. Carroll

June 1979

This report contains results of work carried out for the New York State Energy Research and Development Authority, Albany, New York

Special Report 24
Reference 79-7

Approved for Distribution
J.R. Schubel
J.R. Schubel, Director

ABSTRACT

In this report we have modelled the excess temperature and velocity fields associated with the heated discharge from a large generating station sited on a tidal estuary and used the model, together with appropriate thermal resistance data, to evaluate thermally induced mortality levels of striped bass post yolk sac larvae entrained in the thermal plume of the Consolidated Edision Inc./Power Authority of the State of New York generating facilities on the Hudson River at Indian Point (Units 2&3).

The model consists of separate near-field and far-field portions which were combined to form a complete-field model by vector addition of the velocity fields and by superposition of the excess temperature fields based on a simple mixing concept. By calculating and storing velocity and excess temperature fields appropriate to each of 20 different phases of the tide, our complete-field model follows, and calculates the thermal dose experienced by an assumed initial distribution of passive organisms where the receiving water velocities are time varying, such as occurs in a tidal estuary or coastal setting, as well as unidirectional. For this reason it is considered quasi-transient state.

Application of the model to the cooling water system of Indian Point Units @&3 operating at 873 MWe each[1] and an assumed line of striped bass post yolk sac larvae initially distributed laterally across the river surface upstream from the plant resulted in a list of thermal doses experienced by the larvae ordered with respect to maximum temperature. To evaluate the biological response of the organisms to these doses thermal dose-excess temperature mortality curves appropriate for the 10% mortality level and at acclimation temperatures of 15, 20, and 23°C were constructed for striped bass post yolk sac larvae from data taken by Ecological Analysts, Inc. at their Indian Point field laboratory. A comparison of the maximum calculated thermal dose experienced by any of the plume entrained organisms with these curves indicates that less than 10% of the larvae entrained in the heated plume from Units 2 & 3 will be killed.

The model further suggests that the zone of influence or withdrawal of the intakes is limited to 20-30 meters in the lateral direction.

---

[1] 873 MWe is net rated capacity of Unit 2 and 91% of net rated capacity of Unit 3.

TABLE OF CONTENTS

LIST OF FIGURES

LIST OF FIGURES *(Continued)*

LIST OF TABLES

ACKNOWLEDGEMENTS

We gratefully acknowledge the help during the course of this project of Steven O. Wilson and Carol Hornibrook of the New York State Energy Research and Development Authority. The figures were drafted by Marie Eisel and Carol Cassidy.

Eileen Quinn is due special thanks for typing the many versions of this report.

LIST OF SYMBOLS

A	area of discharge orifice, i.e., $b_o h_o$
A_i	area of intake orifice, i.e., (b-a)H
$A(N)$	a function of N in the conservation of heat relation (eq. (32))
A_r	aspect ratio, h_o/b_o
$B(N)$	a function of N in the conservation of heat relation (eq. (32))
$b(\xi)$	width of jet
c	specific heat of water
D	depth of water
F_r	initial densimetric Froude number $\equiv q_o/\sqrt{\frac{g\Delta\rho_o \bar{h}_o}{\rho}}$
$f(\eta'),f'(\eta')$	lateral shape functions
$g(z'),g'(z')$	vertical shape functions; g may also be the acceleration of gravity
$g''(z)$	vertical scaling factor for $\eta_{\frac{1}{2}}$
$h(\xi)$	depth of jet
H	vertical extent of intake orifice
L	perimeter of jet in η z plane
m	trajectory slope; also mass of small diffusing patch; also sink strength
M	dilution ratio
N	exponent in relation between g" and z'; also release rate of diffusing patches
P	non-dimensional distance $\equiv \frac{D_w}{r_o}\left(\frac{\xi_o}{\xi}\right)^n$
Q	volume flow rate of excess heat or material in jet
Q_R	river flow
$Q'(\tau)$	a function to ensure amount of complete-field excess heat is correct
q	velocity in ξ-direction
R	ratio of initial jet velocity, q_o, to ambient velocity, u_a
R_e	initial Reynolds number $\equiv q_o h_o/\nu$
r_ξ	radius of area equivalent to A_ξ
S	concentration
T	a tidal period, 44712s
t	time
u	x-component of velocity
U_a	tidal velocity amplitude in x-direction
u_a	ambient velocity in x-direction, i.e., $u_a = \bar{u}_a + U_a \sin(\frac{2\pi}{T}t)$
$\bar{u}_a$	mean ambient velocity
v	y-component of velocity
W	width of system
x,y,z	fixed left-handed cartesian coordinate system with x-parallel to shore, y-perpendicular to shore and positive in offshore direction, z directed vertically downward
$z_{\frac{1}{2}}$	half depth of plume (see Figure 5)
ξ,η,z	moving natural coordinate system with positive ξ directed along centerline of jet, η perpendicular to ξ and positive to left of ξ; z directed vertically downward. Origin moves with the peak concentration and is located on the centerline trajectory
α	angle between jet centerline and x-axis
σ	cross-sectional area of river

$2\eta_{\frac{1}{2}}$	half width of jet (see Figure 5)
θ	excess temperature
τ	patch age
ν	kinematic viscosity of water
ω	diffusion velocity
ρ	fluid density
ψ	stream function
μ	surface cooling coefficient
γ	also surface cooling coefficient and equal to $\mu/\rho c$

Subscripts

a	ambient
c	continuous, combined, or complete
f	far-field
i	instantaneous
n	near-field
o	orifice
p	peak or centerline value
$\frac{1}{2}$	where value is one-half of peak value

Superscripts

*	denotes non-dimensional

I. BACKGROUND

In 1977 we described (Carter *et al.*, 1977) a four-step process for evaluating *thermally* induced biological effects due to once-through cooling systems of steam electric generating stations. Our research was prompted by the belief that protecting aquatic life by prescribing some combination of maximum receiving water temperature, maximum temperature rise across the condenser, and maximum size of the mixing zone off the plant, as most regulatory authorities are prone to do, was not well founded scientifically and was potentially misleading. We believed that in order to assess the response of the biota that inhabit the receiving waters to a thermal discharge a method of relating response in "biological units" to stimulus in "physical units" must be found.

Thermal resistance curves, e.g., Figure 1, provide a defensible basis for assessing (or predicting) the thermally induced biological response of organisms exposed to excess temperatures[1] as the result of either pump or plume entrainment. The data (and curves) in Figure 1 are for 50% mortality -- similar curves could be constructed for other mortality levels such as 10%, however. For each acclimation temperature, the length of time that an organism can withstand exposure to an elevated temperature decreases with increasing temperature demonstrating that at least for temperatures ≤ the incipient lethal temperature, thermal death is a dose response. As used here, the thermal dose is defined as

$$\text{Thermal dose} \equiv \int_0^t \theta dt' \qquad (1)$$

where θ is the excess temperature and t is the time of exposure. The incipient lethal temperature is the highest temperature to which an organism can be continuously exposed without increasing the mortality rate. The procedure for calculating doses from thermal resistance curves is described in detail in Section III of Carter *et al.* (1977) and will not be repeated here. It may be assumed at this point, therefore, that for the organism under consideration, the thermal dose has been calculated as a function of temperature (excess temperature + acclimation temperature) from appropriate thermal resistance data for the desired mortality level.

Thermal mixing zones, and hence the spectrum of thermal doses and maximum temperatures experienced by a given distribution of organisms in the receiving waters, are highly site specific. This is so since the fate of heated effluent discharged into a water body depends upon many physical processes which, for purposes of analysis, may be categorized as either *near-* or *far-field* (Figure 2). The near-field processes are governed primarily by the characteristics of the discharge whereas the far-field processes depend on larger scale ambient conditions. Conditions in the near-field are heavily dependent on the thermal emission rate, the initial temperature of the effluent, and the type of discharge. Conditions in the far-field depend on the thermal emission rate, the receiving water characteristics, and surface cooling.

In Carter *et al.* (1977), we showed how off-the-shelf thermal plume models could be combined and exercised to calculate thermal dose as a function of temperature for an assumed distribution of organisms entrained in the heated discharge of a hypothetical generating station with once-through cooling sited on both a river and an estuary. To summarize briefly, we calculated the fields of velocity and excess temperature over space (for both riverine and estuarine cases) and time (the estuarine case only) with the plume models and stored this information. The path or trajectory of each organism of the assumed distribution was then advected with the flow and its trajectory calculated from

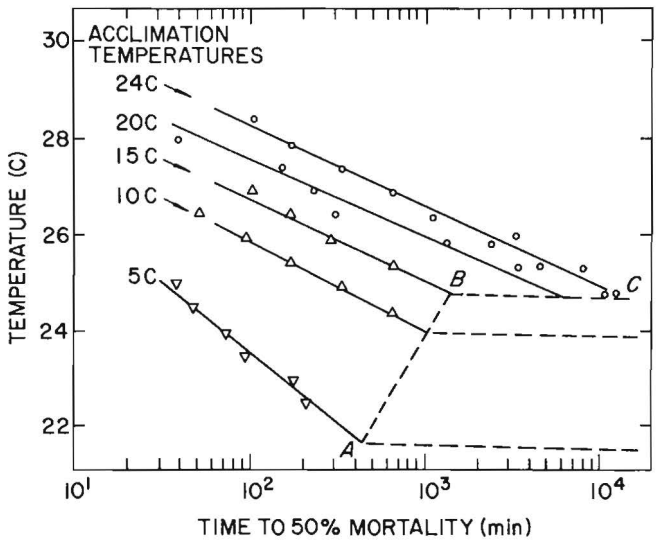

Figure 1. Median resistance times to high temperature of organisms acclimated to different temperatures. For each acclimation temperature there is an incipient lethal temperature -- the highest temperature to which an organism can be continuously exposed for an indefinite period without increasing the mortality rate. Line A-B denotes rising lethal threshold temperatures with increasing acclimation temperature. This rise in threshold eventually ceases at B-C, the *ultimate incipient lethal temperature*. (Adpated from Brett, 1952).

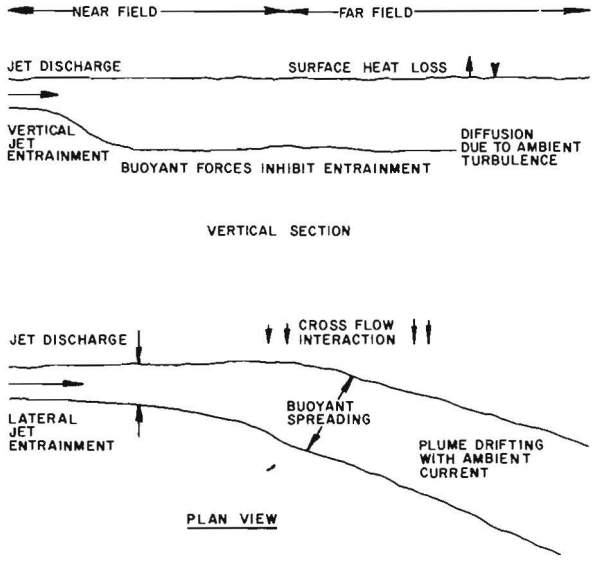

Figure 2. Schematic categorization of plume geometry according to physical processes.

$$x = x_0 + udt, \text{ and} \quad (2a)$$

$$y = y_0 + vdt \quad (2b)$$

where dt is a small interval of time. At each time step, dt, along the path the excess temperature was noted and the integration indicated in equation (1) carried out by the trapezoidal rule. All organisms were followed in this manner until they were no longer exposed to excess heat. The highest excess temperature to which each organism was exposed during its travel was also noted. The result was a list of doses and associated maximum temperatures which was then plotted and compared to a thermal dose versus temperature curve calculated from appropriate thermal resistance data. The relative position of the two curves on a dose-excess temperature diagram (see Figure 3) was then used to determine whether the probability of mortality was greater or less than the mortality level used in developing the thermal resistance curves (50% for the example shown).

The primary objective of this report is to describe a new and improved version of the complete-field thermal plume model and to use it, together with appropriate thermal resistance data, to evaluate mortality levels of striped bass larvae (post yolk sac) entrained in the heated discharge from Units No. 2 & 3 of Consolidated Edison of NY, Inc./Power Authority of the State of New York generating facilities on the Hudson River at Indian Point.

---

[1]Excess relative to acclimation or ambient temperature.

II. MODELING THE FIELDS OF VELOCITY & EXCESS TEMPERATURE

In the previous section we broadly categorized the regions of a thermal plume from a power plant into near- and far-field according to the dominant physical processes, Figure 2. It is important to note, however, that under certain circumstances the two regions interact with important consequences. As pointed out in Carter *et al.* (1977):

> ...in a lake or an estuary where the current reverses periodically due to either wind or astronomical tides, heat discharged at some earlier time (the far-field) may be re-entrained into the jet region (near-field) or directly recirculated into the intake. Periodic interactions of this type can result in variations in the areas enclosed within specific isotherms of several orders of magnitude. Whether or not existing near-field thermal plume models are truly predictive is, therefore, moot other than in a statistical sense, since such models assume that heat leaves the near-field, enters the far-field, and never returns. On the other hand, a far-field model is inadequate to describe conditions in the near-field since it can not account for the effect of the discharge on near-field mixing and flows. In our view, therefore, a combined or complete-field model is required for even a first order estimate of the distribution of excess temperature.

Accordingly, although we will model the near- and far-field separately, we will superimpose and exercise them as an entity, a complete field model.

A. *The Near-field*

In the earlier study we used an existing near-field model known as the Shirazi-Davis model (Shirazi and Davis, 1974). The Shirazi-Davis model is basically the Prych

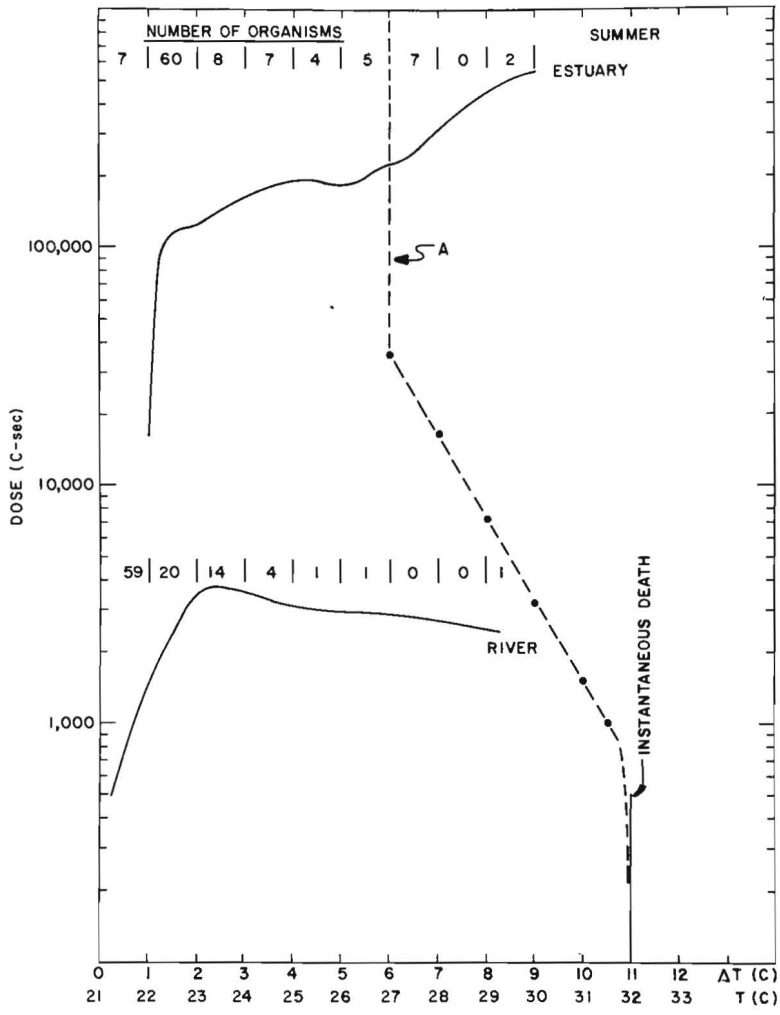

Figure 3. Graphical representation of the Thermal Response Model applied to a New York estuarine/coastal case in summer. The Thermal Dose-Excess Temperature mortality curve (A) was calculated from Thermal Resistance Data and is for a mortality of 50%. The thermal doses experienced by each of the 100 hypothetical organisms are presented for the estuarine and the river cases. The numbers above these curves indicate the number of organisms exposed to the indicated excess temperatures. The probability of mortalities is greater than 0.5 when the thermal dose-maximum excess temperature exposure curve crosses the Thermal Dose-Excess Temperature mortality curve (A). For the riverine case none of the 100 organisms experienced dose-temperature combinations in excess of those associated with a mortality of 50%. For the estuarine case 9 organisms experienced doses in excess of those expected to produce 50% mortality.

model (Prych, 1972) which was calibrated by Shirazi and Davis with available laboratory and field data. The Shirazi-Davis model was selected from the over 40 near-field models that have been formulated because a computer code was readily available and because our interest was limited to demonstrating a concept or idea.

It was our intention at the start of the present research to retain the Shirazi-Davis near-field jet model but to modify it to include an intake. We found, however, in exercising it at various combinations of F_r, A_r, and R, the densimetric Froude number, the aspect ratio, and the ratio of jet velocity to ambient velocity, respectively, that the predicted values of centerline concentration of excess temperature, lateral spread, and vertical growth at various downstream distances compared poorly with measurements made by the senior author (Carter *et al.*, 1974) in a large, low velocity flume at identical values of R, A_r, and F_r. As a result, the Shirazi-Davis model was abandoned and a new near-field phenomenological model constructed with the algorithm's for dilution, lateral spread, vertical growth, and centerline trajectory contained in Carter *et al.*, (1974). Accordingly, pertinent sections of that publication are briefly reviewed below.

1. Measurements of 3-dimensional Heated Surface Jets in a Cross Flow

Parts of this section are essentially repeats of material contained in Carter *et al.* (1974). They are included here for ready reference.

The phenomonon being modeled is shown conceptually in Figure 4. A definition sketch, supplementary to Figure 4, is shown in Figure 5. Previous investigations of heated jets carried out by us and by others such as Jen *et al.* (1966), Hayashi *et al.* (1967), Tamai *et al.* (1969), and Stolzenbach and Harleman (1971) have shown that the dimensionless numbers of greatest import are the Reynolds number, R_e, the densimetric Froude number, F_r, the ratio of initial jet velocity, q_o, to ambient velocity, u_a, and the aspect ratio of the orifice, A_r. They are for the origin or point of discharge.

$$R_e = \frac{q_o h_o}{\nu}$$

where q_o is the inital jet velocity, h_o is the vertical dimension of the orifice and ν is the kinematic coefficient of viscosity,

$$F_r = \frac{q_o}{\sqrt{g \frac{\Delta\rho}{\rho_o} h_o}}$$

where g is the acceleration of gravity, and $\Delta\rho$ is the difference between the density of discharge ρ_o and the density of the receiving waters, ρ_a,

$$R = \frac{q_o}{u_a}$$

where u_a is the velocity of the receiving waters, and

$$A_r = \frac{h_o}{b_o}$$

where b_o is the horizontal dimension of the orifice. Other parameters of importance are, α_o, the angle of discharge measured relative to the x-axis (see Figure 2), the bottom slope, and the surface cooling coefficient. In the measurement program, α_o was maintained at 90°, the depth of water, D, was everywhere constant, and surface cooling was neglected. It can easily be shown that the effect of neglecting surface cooling in the near-field is negligible.

In all except two tests, the Reynolds number was in excess of 3000 such that the jet was fully turbulent and the results independent of R_e. The measurements, therefore, were designed to reveal the dependence of certain characteristics of the heated surface jet on F_r, R, and A_r. The characteristics chosen were (1) the centerline trajectory as defined by the locus of

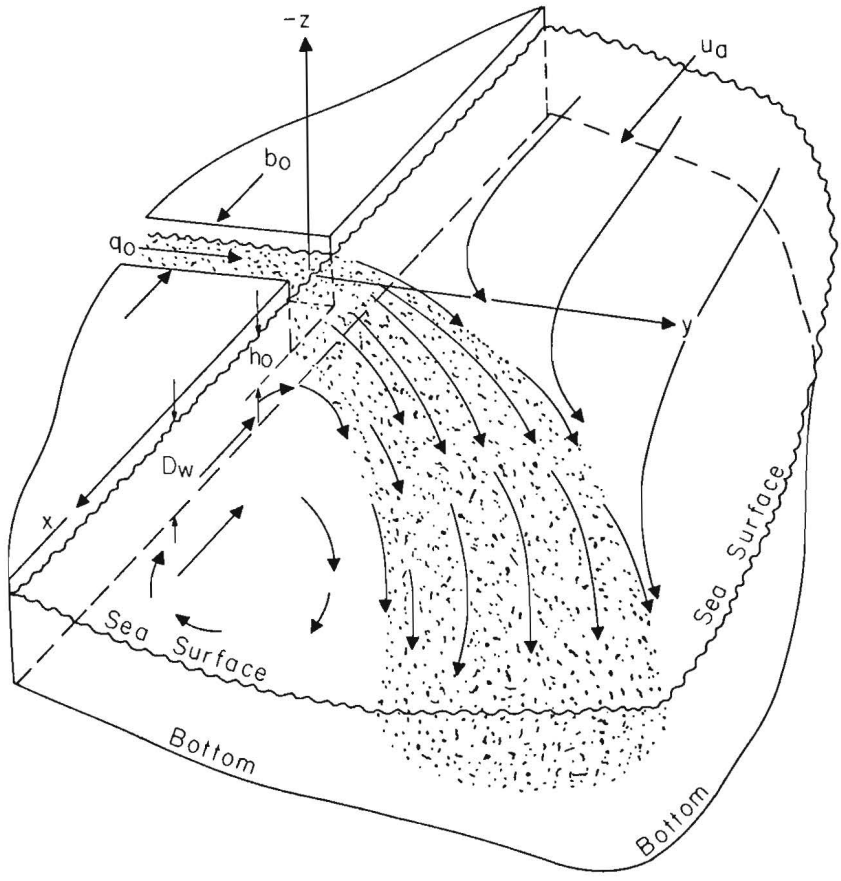

Figure 4. Schematic drawing of a buoyant surface three-dimensional bent-over jet (reprinted from Carter *et al.* (1973)).

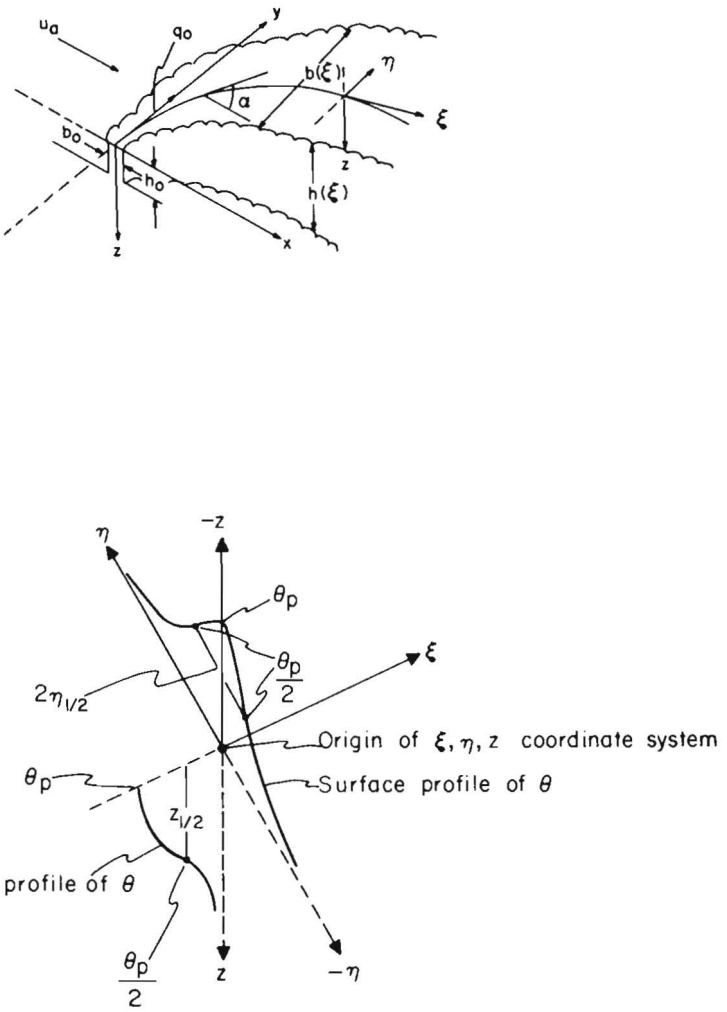

Figure 5. Definition sketches of the three-dimensional heated surface jet in a cross flow.

peak temperatures on the xy plane at z = 0, (2) the depth of the jet as a function of downstream distance, ξ, as defined by $z_{1/2}$, the value of z at which $\theta = \frac{1}{2}\theta_p$ measured on the vertical surface passing through the centerline trajectory, (3) the lateral spread of the jet as a function of downstream distance, ξ, as defined by $2\eta_{1/2}$, the distance measured on the free surface, i.e., z = 0, between the point on the - η axis where $\theta = \frac{1}{2}\theta_p$ and the point on the + η axis where $\theta = \frac{1}{2}\theta_p$, and (4) the dilution, θ_p/θ_o, as a function of downstream distance.

The data were analyzed by collapsing families of curves describing the dependence of a particular characteristic on the various parameters into a single one-dimensional curve by proper scaling. The set of non-dimensional equations arrived at which described the characteristics of a 3-dimensional heated jet in a cross flow were as follows:

Vertical Growth

Initial Zone:

$$\frac{z_{1/2}}{\sqrt{A}} \cdot \frac{1}{A_r^{1/4}} = 0.87 \left(\frac{\xi}{\sqrt{A}}\right)^{1/2} \tag{3}$$

Zone of maximum penetration:

$$\frac{z_{1/2,max}}{\sqrt{A}} \cdot \frac{1}{A_r^{1/4}} = 0.342\ F_r \tag{4}$$

Final zone:

$$\frac{z_{1/2}}{\sqrt{A}} \cdot \frac{1}{A_r^{1/4}} = 0.80\ F_r^{3/2} \left(\frac{\xi}{\sqrt{A}}\right)^{-1/2} \tag{5}$$

The intercept of the initial zone of vertical growth and the zone of maximum penetration is given by

$$(\xi/\sqrt{A})_{IM} = 0.155\ F_r^{\,2}, \tag{6}$$

while the intercept of the zone of maximum penetration with the final zone is given by

$$(\xi/\sqrt{A})_{MF} = 5.472\ F_r. \tag{7}$$

Lateral Spread

Small ξ:

$$\frac{2\eta_{1/2}F_r}{R^2 b_o} = 0.58 \frac{\xi\ F_r}{R^2 b_o} \tag{8}$$

Large ξ:

$$\frac{2\eta_{1/2}F_r}{R^2 b_o} = 2.85 \sqrt{\frac{\xi\ F_r}{R^2 b_o}} \tag{9}$$

The intercept between the lateral spread zone for "small" ξ and that for "large" ξ is given by

$$(\xi/\sqrt{A})_{SM} = 24.145\ (R^2/F_r\sqrt{A_r}). \tag{10}$$

Centerline Trajectory

$$\frac{y}{\sqrt{A}} = R\left(\frac{x}{h_o}\right)^m \tag{11}$$

where $$m = 0.609 - 0.013\ F_r. \tag{12}$$

Dilution

Length of core region:

$$\frac{\xi_o}{\sqrt{A}} = \frac{10.334}{\sqrt{F_r}} \tag{13}$$

Entrainment region:

$$\frac{\theta_p}{\theta_o} = \frac{4.744}{F_r^{1/3}} \left(\frac{\xi}{\sqrt{A}}\right)^{-2/3} \tag{14}$$

Stable region $\left(\frac{z_{1/2,max}}{D} \leq 1\right)$:

$$\frac{\theta_p}{\theta_o} = \frac{1.721}{R^{1/6} F_r^{1/3}} \left(\frac{\xi}{\sqrt{A}}\right)^{-1/3} \tag{15}$$

Stable region $\left(\frac{z_{1/2,max}}{D} > 1\right)$:

$$\frac{\theta_o}{\theta_p} \approx \frac{Q(\xi)}{Q_o}$$

$$= \left\{\frac{1}{P} + \frac{2}{\pi}\left(\ell n \frac{1+\sqrt{1-P^2}}{P} - \frac{\cos^{-1} P}{P}\right)\right\} \tag{16}$$

where $P \equiv \frac{D}{r_o}\left(\frac{\xi_o}{\xi}\right)^{2/3}$, and $r_o = \sqrt{\frac{2A}{\pi}}$.

The intercept between the entrainment region and the stable region for the case ($z_{½,max}/D \leq 1$) is given by

$$(\xi/\sqrt{A})_{ES} = 20.946\ R^{½} \qquad (17)$$

The symbols in the above equations are defined in the text, the List of Symbols, and on Figures 4 & 5. Figures 6, 7, and 8 illustrate the correspondance obtained between the measurements and the equations for lateral spread and vertical growth. For details concerning the analysis, the original reference should be consulted (Carter *et al.*, 1974).

2. A New Phenomenological Near-Field Model

The essential elements of a near-field heated jet model are contained explicitly in equations (3) through (17) with the exception of shape, conservation of heat, and velocity. The velocity is specified implicitly in the centerline trajectory (equations 11 and 12); shape will be specified so as to conserve excess heat.

a. *Velocity.* We assumed that the centerline trajectory determined by flume measurements of the location of the peak excess temperatures at the free surface (z=0) along the plume, and specified by equations (11) and (12), was also a streamline along which a stream function, ψ, would be constant. Therefore, along the centerline

$$d\psi = \frac{\partial\psi}{\partial x}\,dx + \frac{d\psi}{\partial y}\,dy = 0 \quad \text{or}$$

$$\frac{dy}{dx} = -\frac{\partial\psi}{\partial x}/\frac{\partial\psi}{\partial y}. \qquad (18)$$

For incompressible fluids, however,

$$u_p = \frac{\partial\psi}{\partial y}, \text{ and} \qquad (19a)$$

$$v_p = \frac{\partial\psi}{\partial x} \quad \text{or} \qquad (19b)$$

$$\frac{dy}{dx} = v_p/u_p \approx v_p/u_a = \tan\alpha \qquad (20)$$

since $u_p \tilde{\simeq} u_a$ for $\xi/\sqrt{A} \geq R$ (page 31, Carter *et al.*, 1973).

From equation (20) we have that

$$\frac{v_p}{q_o} = \frac{u_a}{q_o}\tan\alpha = \frac{\tan\alpha}{R} \qquad (21)$$

Referring to Figure 9, the centerline component of v_p in the ξ direction can be seen to be $v_p\sin\alpha$ and the centerline component of u_a in the ξ direction $u_a\cos\alpha$. Therefore

$$\frac{q_p}{q_o} = \frac{v_p}{q_o}\sin\alpha + \frac{\cos\alpha}{R} = \frac{\sin^2\alpha}{R\cos\alpha} + \frac{\cos\alpha}{R} \qquad (22)$$

That is, equations (11) and (12) for the centerline trajectory together with equation (20) determines α from which q_p/q_o can be calculated for all $\xi/\sqrt{A}$ with equation (22).

b. *Conservation of Excess Heat.* Discharged heat will be conserved in the receiving waters if the following equation is satisfied

$$\theta_o q_o A = \int_{-\infty}^{\infty}\!\!\int \theta(\xi,\eta,z)\,q(\xi,\eta,z)\,d\eta dz \qquad (23)$$

As is customary, we assumed that although the lateral and vertical distributions of velocity, q, and excess temperature, θ, change with downstream distance, ξ, they retain the same functional forms but with changing scale factors. That is, we assumed

$$\theta(\xi,\eta,z) = \theta_p(\xi)f(\eta/\eta_{½})g(z/z_{½}), \text{ and} \qquad (24)$$

$$q(\xi,\eta,z) = q_p(\xi)f'(\eta/\eta_{½})g'(z/z_{½}) \qquad (25)$$

In Carter *et al.* (1973, 1974) we found that at least for θ, vertical measurements made at $\eta = 0$, i.e., on the centerline, and lateral measurements made at z = 0, the free surface, fit equations (24) and (25) *reasonably* well if

$$f = ½(1 + \cos(\tfrac{\pi}{2}\,\tfrac{\eta}{\eta_{½}})), \text{ and} \qquad (26)$$

$$g = ½(1 + \cos(\tfrac{\pi}{2}\,\tfrac{z}{z_{½}})) \qquad (27)$$

No measurements, however, of f' and g' the

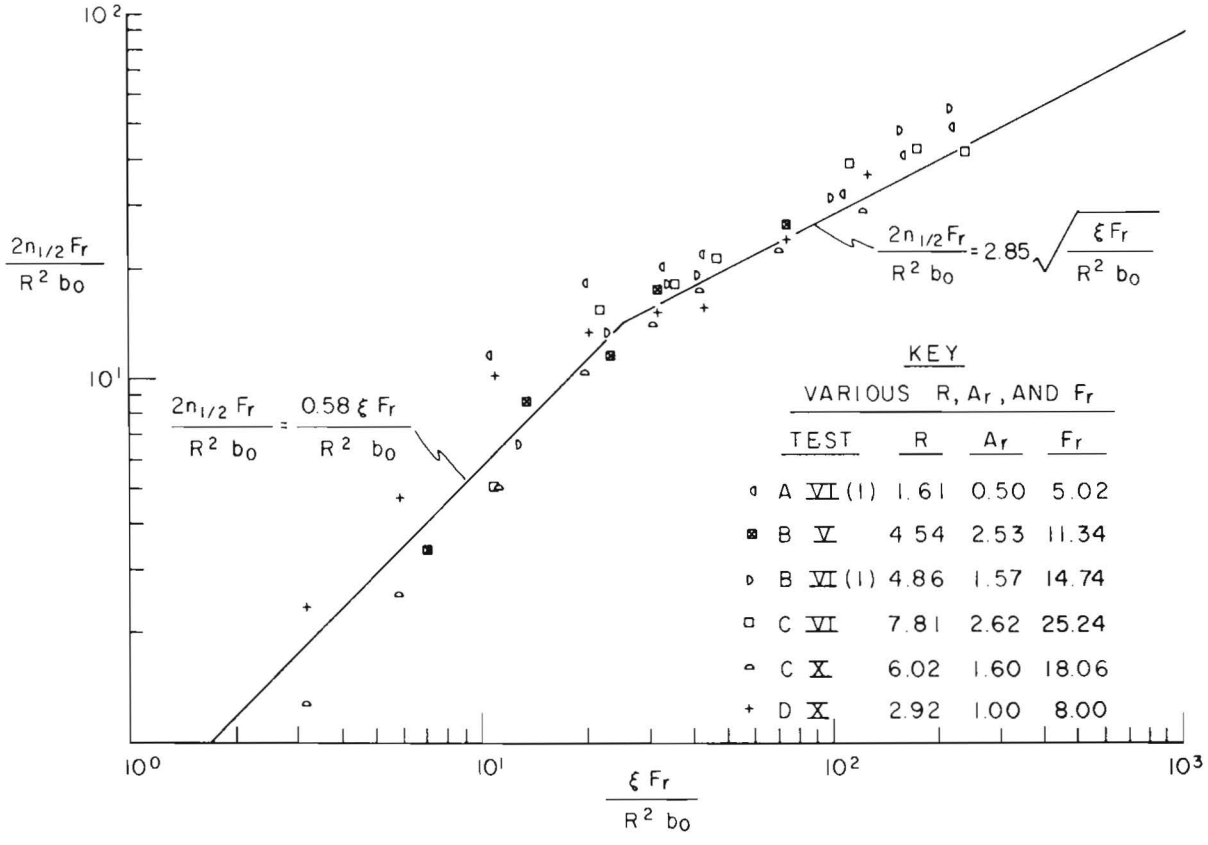

Figure 6. The lateral spread, $2n_{\frac{1}{2}}F_r/R^2b_o$, as a function of downstream distance, $\xi F_r/R^2b_o$, for various R, A_r, and F_r.

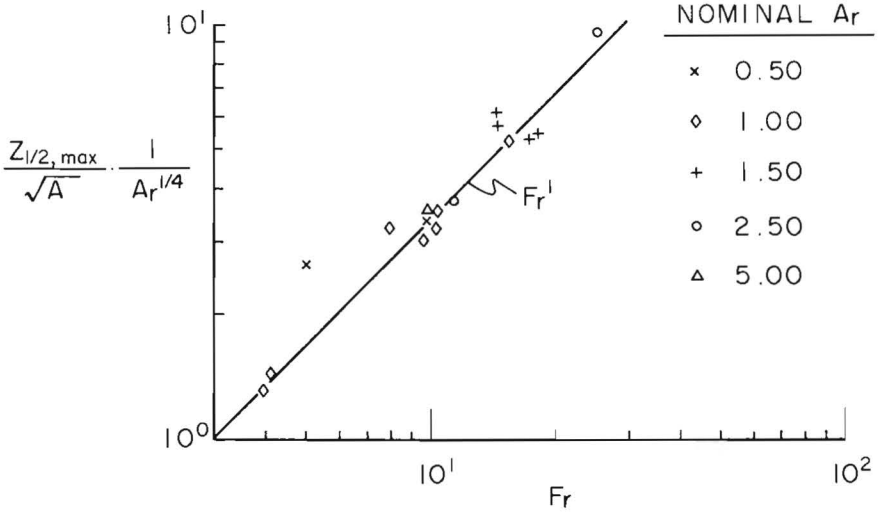

Figure 7. Measured maximum depth, $z_{\frac{1}{2},max}/\sqrt{A}\ A_r^{\frac{1}{4}}$ versus initial densimetric Froude number, F_r.

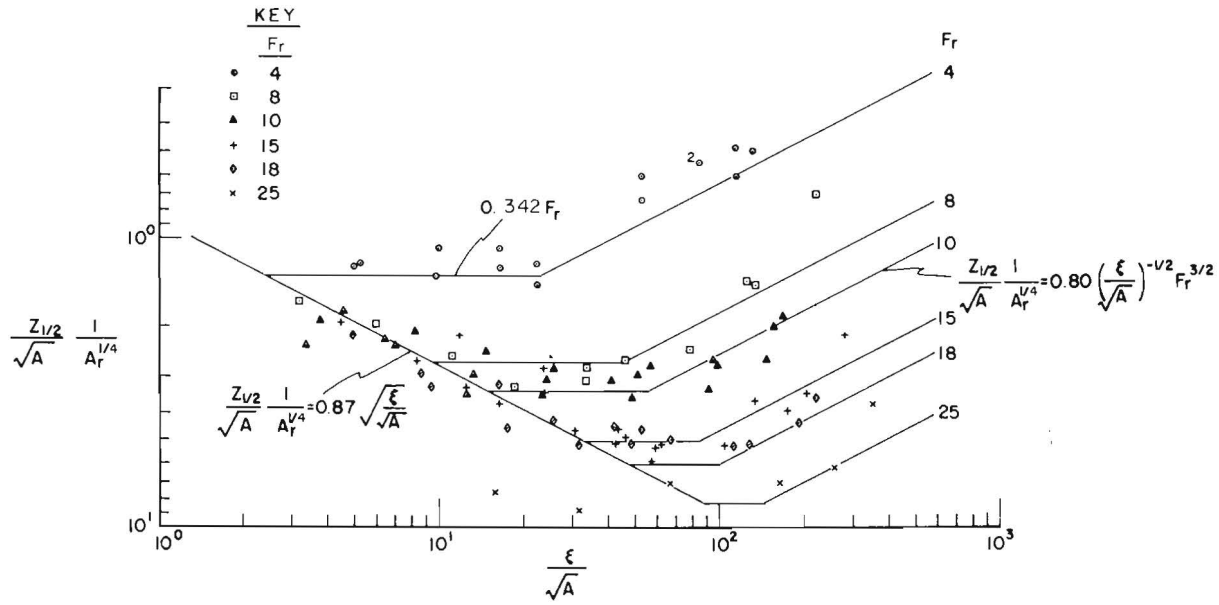

Figure 8. The half depth, as given by $z_{1/2}/\sqrt{A}\ A_r^{1/4}$, versus downstream distance, $\xi/\sqrt{A}$, for various F_r between 4 and 25.

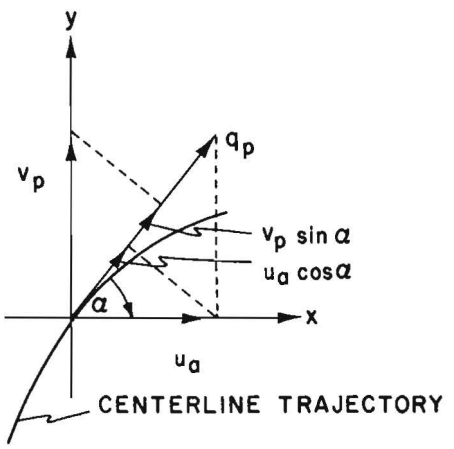

Figure 9. The centerline velocity, q, resolved into its components along the centerline and the x and y axis.

lateral and vertical similarity functions for velocity were made. In the absence of such measurements, we assumed that f = f' and g = g'. Using equations (24-27) then, the RHS of equation (23) was integrated with the result that it was consistently found to be considerably larger than the LHS for a variety of tests and ξ. *Clearly, our model was not conserving excess heat.*

In order to satisfy equation (23) it was necessary to resort to the following procedure. We assumed that

$$f = f' = 1 - 0.5(\eta'/g''(z'))^3, \text{ and} \quad (28)$$

$$g = g' = 1 - 0.5(z')^3 \quad (29)$$

where $\eta' \equiv \eta/\eta_{\frac{1}{2}}$ and $z' \equiv z/z_{\frac{1}{2}}$. That is both $\eta_{\frac{1}{2}}$ and $z_{\frac{1}{2}}$, measured at the free surface and on the plane $\perp$ to the free surface at $\eta = 0$, respectively, were assumed to be functions only of ξ as before but the scaling factor for width, $\eta_{\frac{1}{2}}g''(z')$, was now assumed to vary with z in accordance with the following relation

$$g''(z') \equiv 1 - \left(\frac{z'}{2^{1/3}}\right)^{\frac{1}{N}}. \quad (30)$$

In equation (30), N is a free parameter used to shape the jet's cross section so as to conserve excess heat. It, of course, will vary with ξ. Figures 10, 11, 12, and 13 illustrate for a typical case, the effect of a variable N on the cross section of excess temperature at $\xi/\sqrt{A}$ = 3.325, 10, 52, and 400, respectively.

Equation (23) may now be written as

$$1 = \frac{\theta_p}{\theta_o}\frac{q_p}{q_o}\frac{2\eta_{\frac{1}{2}}}{\sqrt{A}}\frac{z_{\frac{1}{2}}}{\sqrt{A}}\int_0^{2^{1/3}}\int ff'gg'd\eta'dz'. \quad (31)$$

Integrating equation (31) after substitution of equations (28), (29), and (30) yields

$$1 = \frac{\theta_p}{\theta_o}\frac{z_{\frac{1}{2}}}{\sqrt{A}}\frac{2\eta_{\frac{1}{2}}}{\sqrt{A}}\left(B(N)\frac{\sin^2\alpha}{R\cos\alpha} + A(N)\frac{\cos\alpha}{R}\right) \quad (32)$$

where

$$A(N) = 0.8920\left\{\frac{1+5N}{1+5N+4N^2}\right\}, \text{ and} \quad (33)$$

$$B(N) = 0.6560\left\{\frac{1+12N+39N^2}{1+12N+39N^2+28N^3}\right\}. \quad (34)$$

To summarize, our near-field heated jet model is now completely specified for a given set of initial values of R, A_r, and F_r. Equations (3) through (17) determine the centerline trajectory (x,y, and α as functions of ξ), and the jet's lateral spread ($2\eta_{\frac{1}{2}}(\xi)$), vertical growth ($z_{\frac{1}{2}}(\xi)$), and dilution (θ_p/θ_o) along this trajectory; velocities (q_p/q_o) along the centerline are determined by equations (11), (12), (20), and (22). Excess temperatures and velocities normal to the centerline trajectory in the η and z directions are distributed with the aid of equations (28), (29) and (30) after N has been specified along the trajectory by means of equations (32), (33), and (34).

B. *The Far-field*

In our previous study, we treated the far-field by superimposing a large number of small diffusing patches, each from an infinitesimal, instantaneous source and all moving with a velocity, $u_a(t)$. For the diffusion relative to the center of mass for these elementary patches, we chose the Okubo-Pritchard (O-P) diffusion model (Okubo and Pritchard, unpublished note in Pritchard {1960}). This model is one of a class of radially symmetric solutions for horizontal diffusion from an instantaneous vertical line source characterized by a "diffusion velocity." The O-P model is based on the intuitive concept that the rate of change of local variance, i.e., the diffusivity, depends on a characteristic velocity, ω, and the time of diffusion. We recognize that in a turbulent environment the shape of an instantaneous release of material is seldom if ever circular and that by characterizing the velocity field as

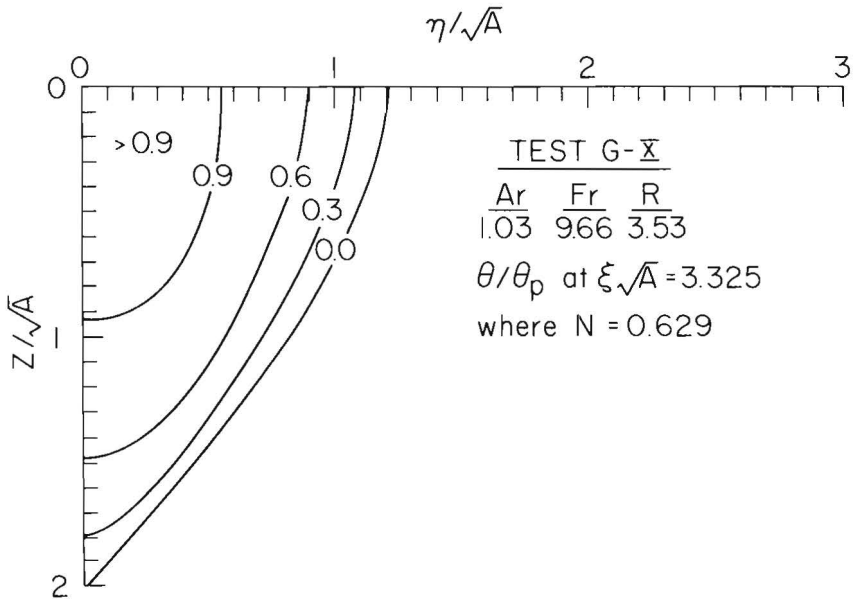

Figure 10. The distribution of excess heat in the ηZ plane necessary to conserve heat at $\xi/\sqrt{A}$ = 3.325 for A_r = 1.03, F_r = 9.66, and R = 3.53. N = 0.629.

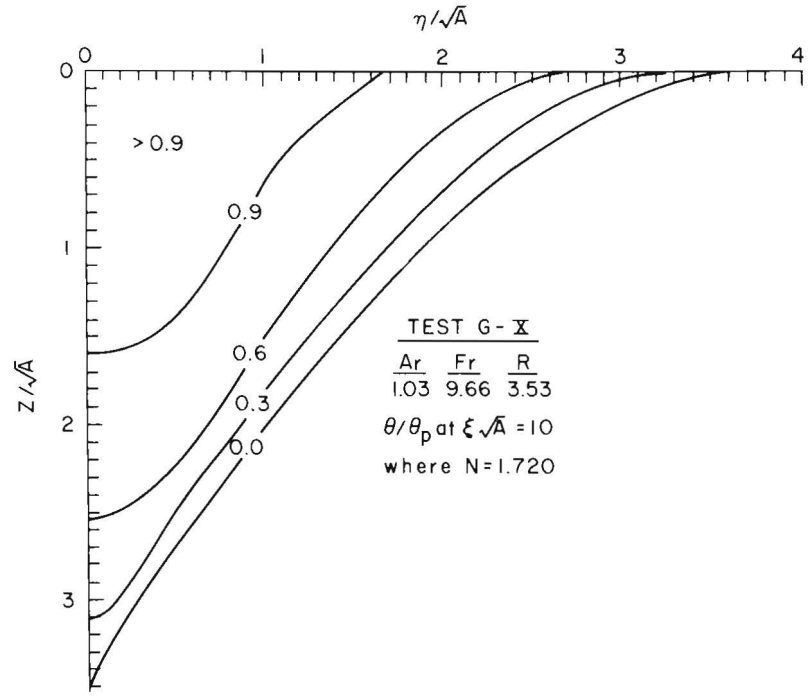

Figure 11. The distribution of excess heat in the ηZ plane necessary to conserve heat at $\xi/\sqrt{A}$ = 10 for A_r = 1.03, F_r = 9.66, and R = 3.53. N = 1.720.

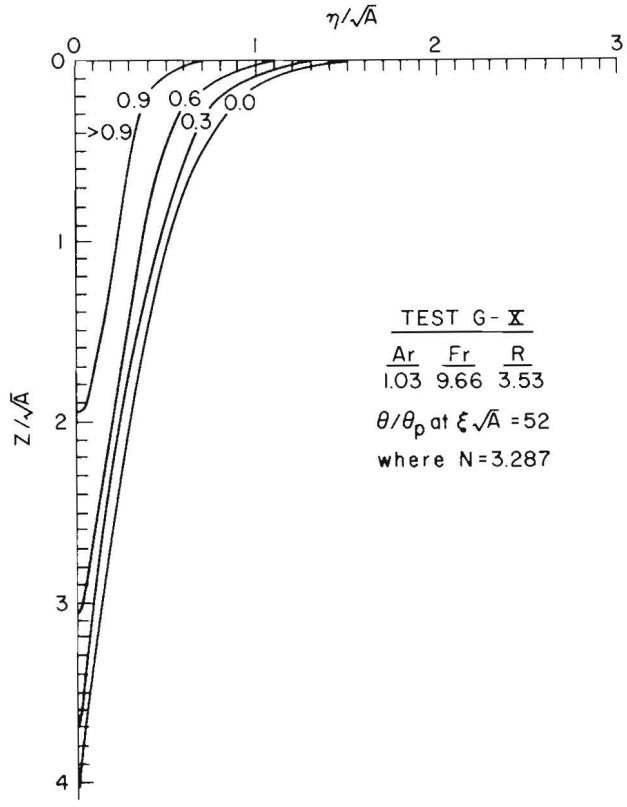

Figure 12. The distribution of excess heat in the ηZ plane necessary to conserve heat at $\xi/\sqrt{A} = 52$ for $A_r = 1.03$, $F_r = 9.66$, and $R = 3.53$. $N = 3.287$.

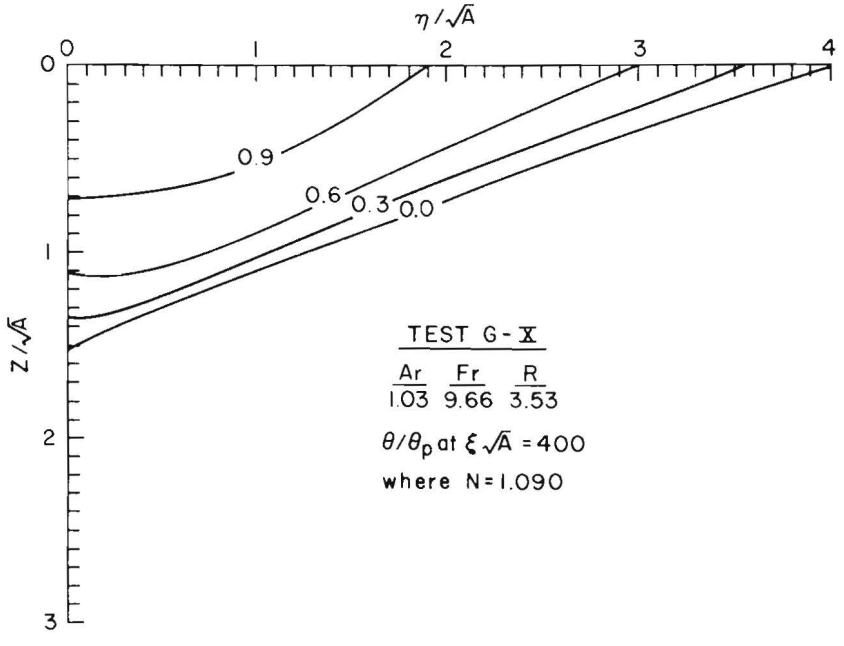

Figure 13. The distribution of excess heat in the ηZ plane necessary to conserve heat at $\xi/\sqrt{A} = 400$ for $A_r = 1.03$, $F_r = 9.66$, and $R = 3.53$. $N = 1.090$.

spatially uniform we cannot account for the highly variable trajectories taken by the various patches. Nevertheless, radially symmetric models have achieved considerable success in predicting the diffusion of introduced substances.

For horizontal diffusion from an instantaneous vertical line source, Okubo and Pritchard proposed the relationship

$$S_i(x,y,t) = \frac{m}{\pi\omega^2 D t^2}$$

$$\exp\{\frac{-(x - \int_0^t u_a(t')dt')^2 - y^2}{\omega^2 t^2}\} \qquad (35)$$

where $S_i(x,y,t)$ is the concentration of material at distance x from the source and y from the centerline, at time t since the single instantaneous release of mass m, distributed uniformly within a layer of thickness D; ω is the diffusion velocity, and $u_a(t)$ the ambient velocity -- assumed to be vertically uniform and directed parallel to the x-axis.

Assuming that a continuous source can be considered as a superposition of a large number of instantaneous releases (N per unit time), we have a time t after initiation of discharge

$$\int_0^t S_i N dt = S_c(x,y,t) = \frac{Q}{\pi\omega^2 D} \int_0^t \frac{1}{\tau^2}$$

$$\exp\{\frac{-(x - \int_{t-\tau}^t u_a(t')dt')^2 - y^2}{\omega^2\tau^2}\}d\tau \qquad (36)$$

where $S_c(x,y,t)$ is now the concentration from a continuous release of material at the rate Q=Nm and is made up of patches whose age, τ, varies from 0 to t.

For the simple case where u_a is constant, equation (36) may be integrated analytically with the result that

$$S_c(x,y,t) = \frac{Q}{2\sqrt{\omega}\ \omega D\ \sqrt{x^2+y^2}}$$

$$\exp\{-\frac{u_a^2\ y^2}{\omega^2(x^2+y^2)}\}\{1-\mathrm{erf}(\frac{\sqrt{x^2+y^2}}{\omega}[\frac{1}{t} - \frac{xu_a}{x^2+y^2}])\} \qquad (37)$$

For the more general estuarine/coastal situation where u_a is a function of t, the integration of equation (36) in its present form cannot be carried out analytically; in our previous study it was performed numerically. Due to τ^2 appearing in the denominator of the integral, however, very small time steps had to be taken with the result that computation time became excessive and the result erratic. It can be integrated analytically, however, by approximating the integral of the time dependent portion of u_a between the limits t-τ and t.

First, replace $S_c(x,y,t)$ by θ, the excess temperature, and $u_a(t)$ by $\bar{u}_a+U_a\sin(\frac{2\pi}{T}t)$. Define Q as $\theta_o q_o A$, the source heat flux. After these substitutions, equation (37) becomes

$$\frac{\theta}{\theta_o} = \frac{Q}{\theta_o\pi\omega^2 D} \int_0^t \frac{1}{\tau^2}$$

$$\exp\{\frac{-(x-x_o-\int_{t-\tau}^t (\bar{u}_a+U_a\sin(\frac{2\pi}{T}t'))dt')^2}{\omega^2\tau^2}\}$$

$$\exp-(\frac{y-y_o}{\omega\tau})^2\, d\tau \qquad (38)$$

where x_o,y_o is the location of the heat source. Equation (38) in non-dimensional form is

$$\theta^* = \frac{Q^*}{\pi} \int_0^{t^*} \frac{1}{\tau^{*2}} \exp-(\frac{U_a}{\omega})^2$$

$$\{\frac{x^*-x_o^*+\bar{u}_a^*\tau^* + \int_{t^*-\tau^*}^{t^*} \sin(2\pi t^{*\prime})dt^{*\prime})}{\tau^*}\}^2$$

$$\exp-(\frac{U_a}{\omega})^2(\frac{y^*-y_o^*}{\tau^*})^2 d\tau^* \qquad (39)$$

where

$$x \equiv U_a T x^*,\ y \equiv U_a T_y y^*,\ t \equiv Tt^*,\ \tau \equiv T\tau^*,$$

$$\bar{u}_a \equiv U_a\bar{u}_a^*,\ U_a \equiv U_a U_a^*,\ \theta \equiv \theta_o\theta^*,$$

$$\text{and } Q \equiv \theta_o\omega^2 DT\ Q^*.$$

Next, the time dependent part of u_a in equation (39) was integrated by replacing

$\sin(2\pi t^{*\prime})$ with a square wave of amplitude $2/\pi$, the mean of $\sin(2\pi t^*)$. On integration, a saw-tooth function resulted which was exactly equivalent to $\int_{t^*-\tau^*}^{t^*} \sin(2\pi t^{*\prime})dt^{*\prime}$ at $t^*=0$, ¼, ½, ¾, 1, ... $\frac{k-1}{4}$ and an acceptably close approximation everywhere else. As a result of this approximation, the individual patches are moved somewhat faster or slower during the tidal cycle at times which depend on the value of τ^*, the patch age, but are all positioned correctly every quarter-tidal cycle.

After this simplification, the exponential arguments in equation (39) were squared as indicated and the RHS replaced by the sum of a series of integrals, each taken over a flood or ebb phase or portion thereof. On their integration, now possible, a series of error functions resulted. For details of our treatment of equation (39), see Wilson (1979).

Ultimately, of course, all excess heat discharged to the receiving waters in the cooling water from a generating station must be rejected to the atmosphere by the processes of long wave back radiation, evaporation, and conduction. The rate of change of excess temperature of a small patch as a result of these processes has been shown to be exponential (Gameson *et al.*, 1959; Pritchard *et al.*, 1965) and expressable in the form

$$\left[\frac{\partial\theta}{\partial t}\right]_{\text{cooling}} = \frac{\mu\theta}{D\rho c} = \frac{\gamma\theta}{D}, \quad \text{or}$$

$$\theta/\theta_o = \exp\{-\frac{\gamma\tau}{D}\} \qquad (40)$$

where γ is $\mu/\rho c$, μ the surface cooling coefficient, and ρ and c are the density and specific heat, respectively, of water. μ has been tabulated by Pritchard (unpublished) in BTU/(f^2 °F h) as a function of wind speed, θ, and ambient water temperature. For the continuous discharge case, however, the RHS of equation (40) must be included in equation (39) but inside the $\int_0^{t^*}$ since we require a model which includes far-field surface cooling. In this form, however, equation (39) is no longer integrable. To evaluate it, we followed the procedure described in the previous section but reduced the limits of integration from ½ tidal cycle (flood or ebb) to 1/100 of a tidal cycle and replaced $\exp(-\gamma\tau/D)$ inside each integral with its mean value outside the integral. For computation, $\exp(-\gamma/D\tau)$ was non-dimensionalized as $\exp-(\frac{\omega}{U_a})(-\gamma^*\tau^*/D^*)$ where $\gamma^* \equiv \gamma/\omega$, and $D \equiv U_a T\ D^*$.

C. *Superposition of the Near and Far-fields into the Complete-field*

For our complete-field model we simply superimposed the near- and far-field velocities and excess temperatures. The two temperature fields, one from the near-field model and one from the far-field model, were superimposed in accordance with the following simple mixing concept.

Let $\theta_n(x,y,z,t)$ be the excess temperature resulting from the near-field model, $\theta_f(x,y,z,t)$ be the excess temperature resulting from the far-field model, $\theta_c(x,y,z,t)$ be the excess temperature resulting from the combined fields, and θ_o be the excess temperature at the point of discharge, then, for the case where $\theta_f > 0$, the combined excess temperature at any point x, y, z, and time t is given by

$$\theta_c(x,y,z,t) = \frac{1 \cdot \theta_o + M \cdot \theta_f(x,y,z,t)}{1 + M} \qquad (41)$$

if we neglect surface cooling. In equation (41), M is the volume into which a unit volume at temperature θ_o is considered to be mixed. Similarly, for the case where $\theta_f = 0$,

$$\theta_n(x,y,z,t) = \frac{1 \cdot \theta_o}{1 + M} \qquad (42)$$

Rearranging equation (42), we have

$$M = \frac{\theta_o}{\theta_n} - 1. \qquad (43)$$

Finally, substituting equation (43) into (41) results in

$$\frac{\theta_c}{\theta_o} = \frac{\theta_n}{\theta_o} + \left(1 - \frac{\theta_n}{\theta_o}\right) \frac{\theta_f}{\theta_o} \qquad (44)$$

which is the desired superposition scheme for excess temperature.

As described in the previous section, the far-field model includes all the excess heat that has been rejected since t=0. Upon superposition, this must be reduced so that the total amount of excess heat in the complete-field will be correct. That is, heat added in the near-field must be removed from the far-field or

$$\{\iiint_{V(\xi)} \theta_n \, d\eta \, dz \, d\xi\}_{\substack{\text{near-field} \\ \text{addition}}} = \{Q \int_0^{\tau_1} Q'(\tau) \, d\tau\}_{\substack{\text{far-field} \\ \text{removal}}} \qquad (45)$$

Where $Q'(\tau)$ is a function that reduces from 1 to 0 between $\tau=\tau_1$ and $\tau=0$ so that equation (45) is satisfied (Fig. 14). In other words, at $\tau=\tau_1$, i.e., time $(t-\tau_1)$ after initiation of the discharge, the heat rejection rate Q is made to die away so that the heat added in the near-field is removed from the far-field. This has been accomplished by reducing the strength of the parcels of excess heat most recently discharged, i.e., ages between 0 and τ. We found that for a range of R, i.e., tidal phases, equation (45) is satisfied within a few percent if $Q'(\tau) = \frac{1}{2}(1 \cos \frac{2\pi\tau}{1.6T})$, $\tau_1 = 0.8\tau$, and if the superposition is truncated at $\xi/\sqrt{A} = 100$.

Since Q* in equation (39) is now a function of τ^*, it must be moved inside the $\int_0^{t^*}$ and treated identically to the surface cooling term in the integration of (39).

The two velocity fields, one due to the heated discharge and the other to the ambient flow, can be combined by simple vector addition as described earlier in Section II C (p.). That is, q_p, the centerline or peak velocity in the ξ direction is given by the sum of $v_p \sin \alpha$, due to the near-field, and $u_a \cos \alpha$, the ξ-component of the ambient or receiving water flow (Fig. 9). This result, however, does not take into account the influence, if any, of the plant's intake. In a once-through cooling system, water must be drawn in at the same rate it is discharged. The inclusion of an appropriate intake may, therefore, modify the results of any velocity superposition scheme which does not take its effect into account. Its effect, if any, will depend upon its character and location.

We chose to treat the intake as a line sink of strength $m = Q/H$ where H is the vertical extent or depth of the intake. According to Milne-Thomson (1960), the motions due to such a sink are given by $-(Q/A_i) \ln \sqrt{\frac{(x-a)^2+y^2}{(x-b)^2+y^2}}$ in the x-direction and $(Q/A_i) \ln\{\tan^{-1}(\frac{y}{x-a}) - \tan^{-1}(\frac{y}{x-b})\}$ in the y-direction where A_i is the area of the rectangular intake orifice whose corners are located at (b,o,o), (a,o,o), (b,o,H), and (a,o,H). These components must be added to the x and y components of the ambient flow, $u_a(t)$ and o, respectively, prior to superposition with the velocities due to the plant's discharge. Such a procedure accounts, at least to a first approximation, for the effect of the intake. It can be easily shown that the inward velocities in the neighborhood of the intake are inversely proportional to the distance off-shore from the intake. As a result, the region influenced by the intake is relatively small unless A_i is small, i.e., large intake velocities.

III. APPLICATION OF THE COMPLETE-FIELD MODEL TO A GENERATING STATION IN NEW YORK STATE WATERS

In the previous sections we developed a new thermal plume model with which we could 1) calculate time-excess temperature histories experienced by organisms entrained in the plume, and 2) obtain the thermal doses (°C-sec), ordered with respect to maximum excess temperature,

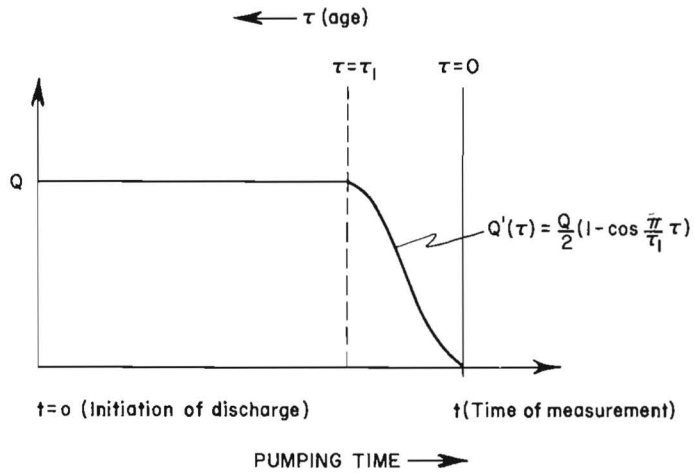

Figure 14. The source term, $Q'(\tau)$, for the far-field model as a function of age (τ) or pumping time (t) such that heat added in the near-field is removed in the far-field.

experienced by these organisms by integration of their time-excess temperature histories. We also described how this list of doses could be used together with appropriate thermal resistance data to evaluate mortality levels of the entrained organisms. In this section we shall apply our model to the Indian Point generating facilities (Units 2 & 3) operated by Consolidated Edison of NY, Inc./Power Authority of the State of NY on the Hudson River.

A. *A Description of the Computational Routines*

In order to apply the model, a segment of the Hudson River off Indian Point, 10,759 m long by 1537 m wide, was schematized with a 71 by 11 array of square elements, 153.7 m on a side (the coarse grid). The near-field was further subdivided into a fine grid consisting of a 49 by 41 array of square elements, 1/8 the size of the coarse grid elements. The discharge was located at (21,1) on the coarse grid and (25,1) on the fine grid. Thus the fine grid (1920 elements) overlayed 30 coarse grid elements, 5 elements in the y-direction and 6 elements in the x-direction.

With appropriate values of F_r, A_r and R specified, 20 sets of jet computations were carried out along the jet centerline (ξ^*) for times between 6.00 and 6.95 tidal cycles (12.42 hours) in steps of 0.05 tidal cycles, each of which contained all the parameters necessary to compute the jet velocity and near-field excess temperature at any given point off the centerline (θ^*, x^*, y^*, $2n_{\frac{1}{2}}^*$, $z_{\frac{1}{2}}^*$, α, N, and A(N)).

Next, a set of 20 each coarse and fine grid excess temperature fields for the far-field were calculated for the same values of t* after assigning appropriate values of Q, ω, $u_a(t)$ and D, and *merged* (superimposed) with the previously computed near-field values in accordance with equation (44).

These data, together with the x and y coordinates of each organism in the assumed initial distribution, were the required inputs to the organism tracking/dose programs. The tracking program was arranged so that all organisms were moved, in succession, a coarse time step ($\Delta t^* = 0.05$). This time step was restricted, however so that an organism could not move more than one grid unit (coarse or fine) in either the x or y direction. As an added restriction, a buffer zone of one coarse grid was placed around the fine grid. In this zone, the coarse grid temperature fields were used but movement was restricted to a maximum of one fine grid. This prevented moving an organism an excessive distance on entry into or departure from the fine grid.

At each time step, the excess temperature was computed appropriate for its position using a linear interpolation in time between 4-point spatial interpolations from the last and for the next coarse times. The velocity at the current position, including the ambient and intake contributions, was also computed similarly by linear interpolation in time using the data previously stored along and off the jet centerline together with the algorithms for the intakes (Section II C) and the ambient flow, i.e., $u_a(t) = \bar{u}_a + U_a \cos \sin(2\pi t^*)$.

New positions were then calculated using these velocities and the minimum of a) the time step necessary to move one grid unit in the x-direction, b) in the y-direction, or c) to the next coarse time.

It may be seen from the foregoing that each organism was incrementally moved in succession until it had undergone one coarse time step. Then the next set of data inputs were loaded and the process repeated until such time as all organisms were outside the influence of the heated plume. This was considered to occur when the organism remained outside the coarse grid one full tidal cycle. Organisms carried out of the coarse grid and later returned, were tracked during the time they were outside the coarse grid but were assumed to experience an

excess temperature equal to the mean of their exit and reentry temperatures.

Doses were then computed in accordance with equation (1) using the trapezoidal rule and ordered with respect to the maximum excess temperature experienced.

B. *The Indian Point Generating Facilities.*

The Indian Point Station is located on the east bank of the Hudson River about 25 miles north of the New York city limits. It consists of three units - Unit 1 rated at 265 MWe (not operated since October 1, 1974), Unit 2 rated at 873 MWe (operated since September 28, 1973), and Unit 3 rated at 965 MWe (operated since August 30, 1976). All three units utilize pressurized light-water nuclear reactors. Since Unit 1 is not operating at present, we shall confine our description of these facilities to Units 2 & 3.

Steam generated by the reactors drives tandom-compound turbine-generator units. The turbine assemblies, essentially identical for Units 2 & 3, consist of one high-pressure and three low-pressure turbines on a single shaft. Each low-pressure turbine exhausts into a separate single-pass condenser cooled by water from the Hudson River (once-through). For every kilowatt of electricity produced, approximately 2 kilowatts of heat (239 calories/sec) must be rejected to the environment (~ 30% efficiency). At Indian Point this is accomplished by means of a once-through cooling system. Cooling water is drawn from the river past trash bars and intake screens, through the pump bay and circulating water pumps, the condenser water boxes and condensers, and then returned to the river via a common discharge canal to a 12 port discharge structure located approximately 190 m (620') downstream from Unit 3 intake. The overall plant arrangement is shown in Figure 15. openings - six openings 4.07 × 7.93 m (13'4" × 26') for condenser cooling water and a single, smaller opening for service water. The top of each opening is located at -1.0' below mean sea level (MSL) to retain floating debris and ice. Each of the six larger openings is serviced by a single 140,000 gpm (8.83 m^3s^{-1}) pump and the service water opening by six 5,000 gpm (0.32 m^3s^{-1}) pumps for a total withdrawal of 870,000 gpm (54.88 m^3s^{-1}) per unit.

Units 2 and 3 use a common discharge structure whose centerline is located approximately 191 m (627') from the centerline of Unit 3 and 400 m (1312') from the centerline of Unit 2. Figure 16 is a schematic of the structure. As may be seen in Figure 16, the heated cooling water is discharged to the river at depth through a series of ports, 12 in all, 4 feet high × 15 feet long (~ 1.22 m × 4.57 m), located on 21 foot (6.40 m) centers. Ten of the ports are provided with adjustable gates that can be raised or lowered to maintain the velocity of discharge at 10 f s^{-1} (3.05 m s^{-1}). The centerline submergence of the ports is 12 feet (3.66 m) below MSL. The excess temperature of the existing discharge water is 8.5 C°(15.3°F) over ambient. For a flow of 1,740,000 gpm (109.8 m s^{-1}), and a river temperature of 20°C (68°F), the densimetric Froude number of the discharge is 18.8. The structure's aspect ratio, A_r, and cross sectional area, A, for a discharge velocity of 10 f s^{-1} (3.05 m s^{-1}) are 0.03 and 49.57 m^2 (533.33 f^2), respectively.

C. *Results*

1. The Fields of Excess Temperature and Velocity

In carrying out the thermal dose calculations, we used the following values for the parameters required as inputs to the model:

Near-field Model

$A = 533.3$ f (49.6 m^2)

A_i(Unit 2) = 3120 f (290 m^2)

A_i(Unit 3) = 3250 f (302.1 m^2)

$F_r = 17.48$

$T = 44712$ s

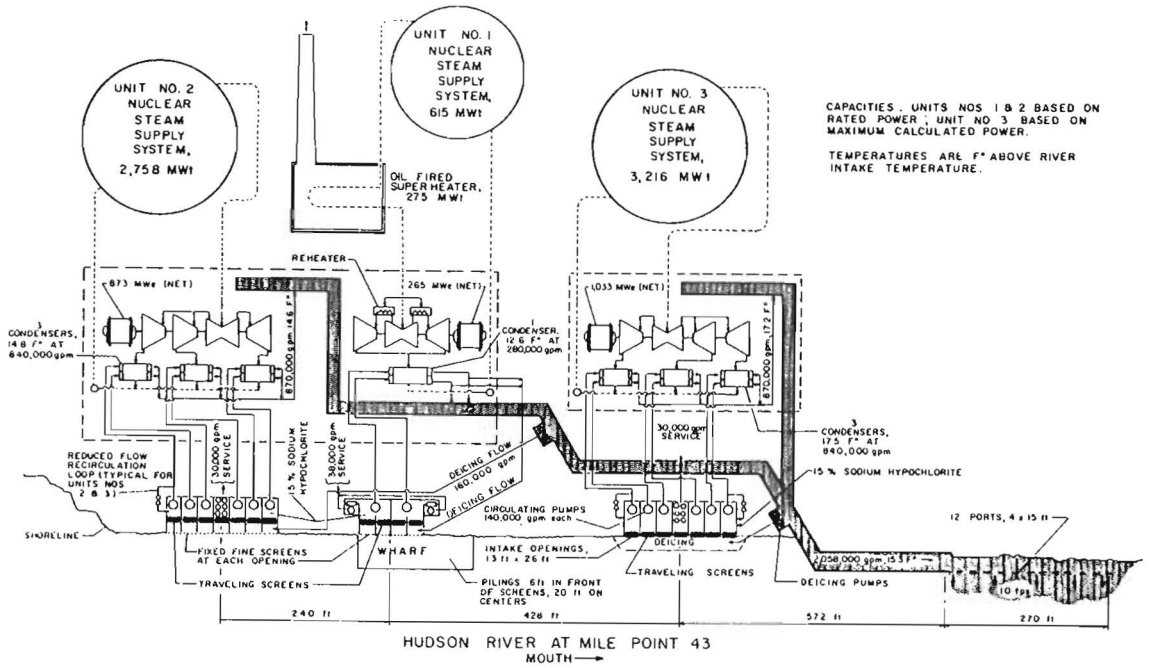

Figure 15. Schematic representation of Indian Point Plant cooling water systems (Source - Consolidated Edison, Inc.).

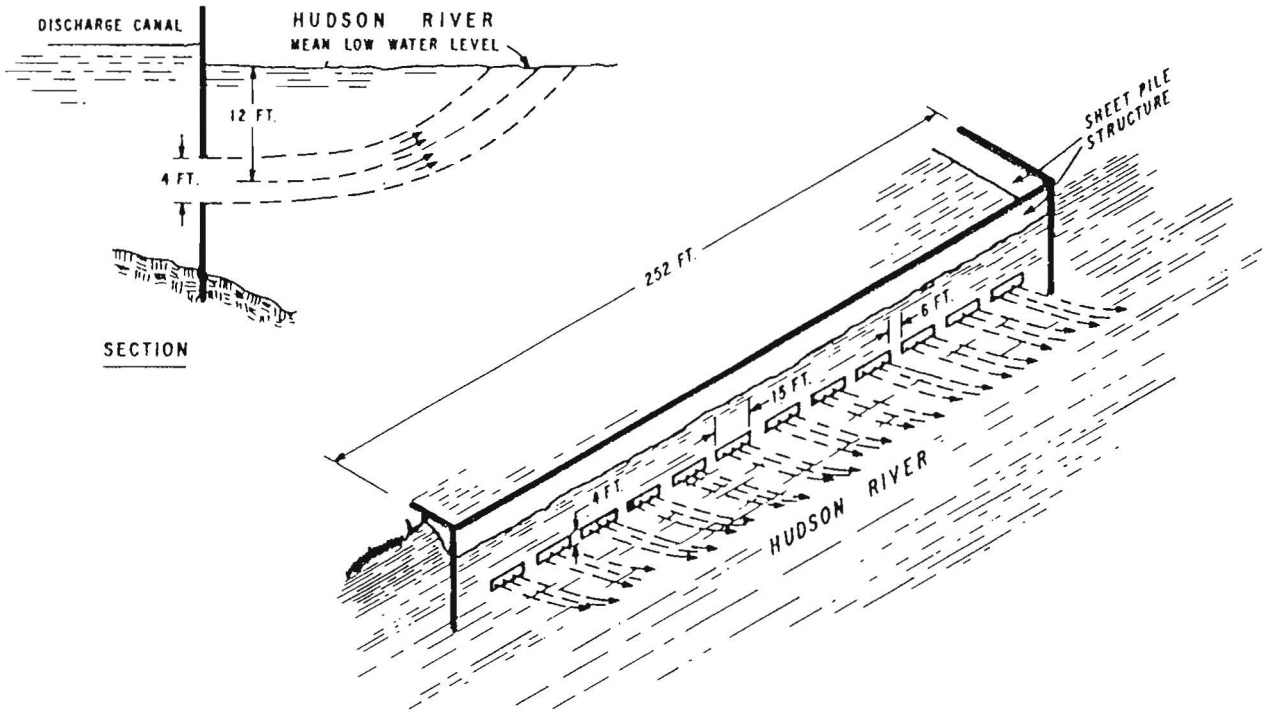

Figure 16. Diagrammatic sketch of Indian Point Discharge Structure (Source - Consolidated Edison, Inc.).

A_r = 0.03

R = 10.1(max. ebb) or
12.78(max. flood)
- 26.49(near slack)

θ_0 = 8.5°C(15.3°F)

q_0 = 10 fs^{-1}(3.05 ms^{-1})

Far-field Model

$\bar{u}_a = 2.5\ Q_r/\sigma$

U_a = 0.27 ms^{-1}

ω = 1.5 $10^{-2} ms^{-1}$

σ = 160,000 f^2(14,872 m^2)

T = 44712s

D = 15 m(4912 f)

γ = $5.6 \times 10^{-6} ms^{-1}$
(100 BTU/(f^2°F day))

Q_R = 6640 cfs(188 $m^3 s^{-1}$)

θ_0 = 8.5°C(15.3°F)

Q_0 = 109.8 $m^3 s^{-1}$

The values tabulated as inputs to the near-field model are obtainable from information provided in Section IIIB, The Indian Point Generating Facilities, and are appropriate for net rated capacity (873 MWe) of Unit No. 2 and 91% of net rated capacity (965 MWe) of Unit No. 3, the current licensed power output levels. F_r, the densimetric Froude number is appropriate for a river temperature of ~ 80°F, i.e., midsummer.

With respect to the far-field values, Q_R is the average of the monthly mean freshwater flows for August at Green Island, N.Y. for the period 1947-1975 increased by 20% to account for the drainage area between Green Island and Indian Point (Table 2-1, Consolidated Edison/PASNY, July, 1977). U_a is the average tidal amplitude according to the same publication and $\bar{u}_a$ is the estimated net non-tidal velocity in the upper 15 meters. It is given by Q_R/σ augmented by the factor 2.5 to account for gravitational convection and/or covariance between tidal elevation and velocity.

The values of ω and D selected were a compromise since they appear in equation (39) as a product, $\omega^2 D$. Therefore an equivalent increase in either ω^2 or D reduces θ at a particular point in space and time by the same amount. To make a selection, we used information on recirculation (Table 1-15, Appendix D to Indian Point Gen. Sta. 316(a) Demonstration) and thermal plume survey data taken in June, 1977 when both Units 2 and 3 were on line and at or near 873 MWe each (Consolidated Edison, 1978). D appears to be somewhat high but we felt that ω should not exceed 1.5 cm s^{-1} based on information from many dye tracer experiments carried out by the senior author in estuaries with similar physical characteristics. Model predictions for recirculation over a typical tidal cycle compared to measured values contained in Table 1-15 of Appendix D to the Indian Point Generating Station 316(a) Demonstration are shown in Figure 17. In addition, the predicted tidally averaged recirculation, 8%, compares very favorably with a value of 7.7% reported in Parkinson and Goulet, 1976 which is based on measurements made in a hydraulic model.

γ, the surface cooling cooefficient is appropriate for a wind speed of 5 mph, a river temperature of 80°F, and a excess temperature of 5°F.

On Figure 18 we show the resulting predicted surface distribution of excess temperature, θ^*, at four different tidal phases, t/T = 6.05 (approximately slack before ebb), 6.25 (maximum ebb), 6.55 (approximately slack before flood), and 6.75 (maximum flood). Figure 19 shows the predicted surface velocity fields for t/T = 6.05 and 6.75.

2. Thermal Dose Calculations.

Ninety (90) organisms, assumed to represent striped bass post yolk sac larvae, were distributed laterally across the river at the surface, 20 coarse grid intervals [3,074 m (10,082.7 f] upstream from the centerline of the discharge. The first eighty-one (81) of these organisms were placed every 9.61 m (31.5 f); the remaining nine (9) were located at intervals of 76.9 m (252 f). All were tracked, doses computed, and the maximum excess temperature, θ^*, noted as outlined in Section IIIA. The

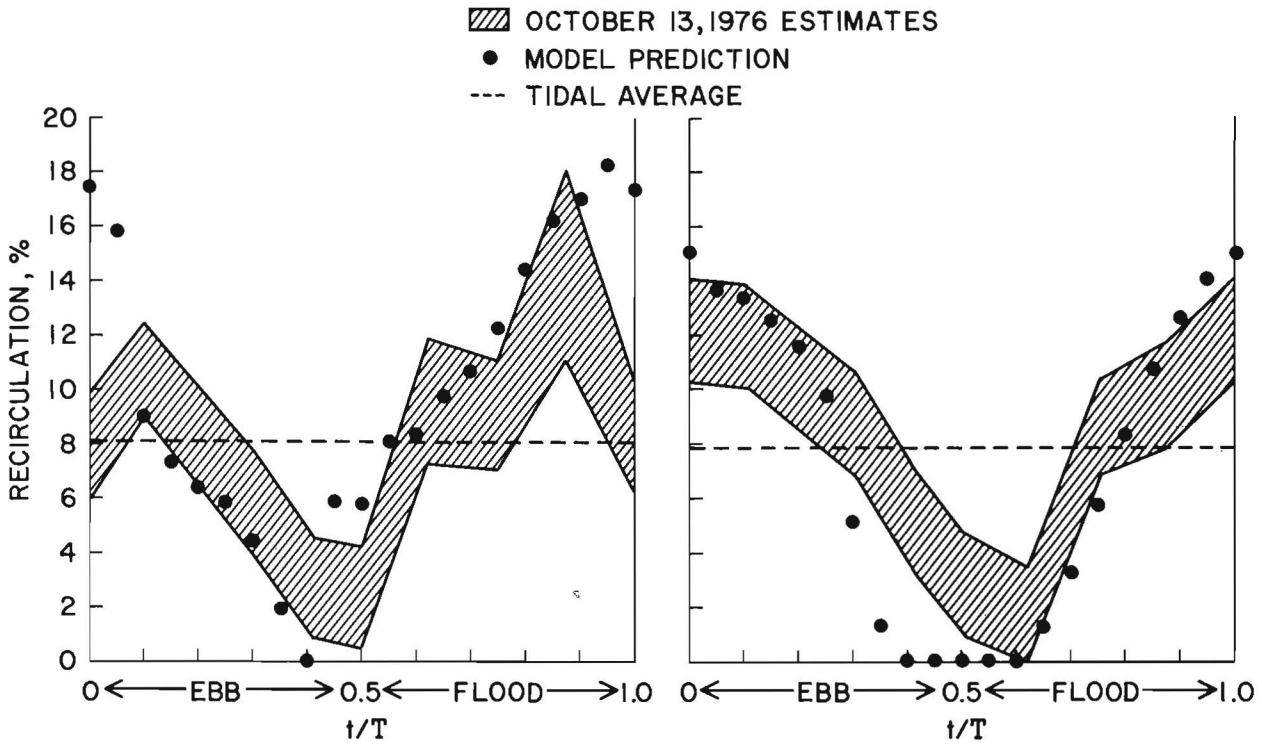

Figure 17. A comparison of the recirculation predicted by the MSRC Complete Field Thermal Model for Indian Point Units 2 and 3 and values measured by Consolidated Edison on 13 October, 1976.

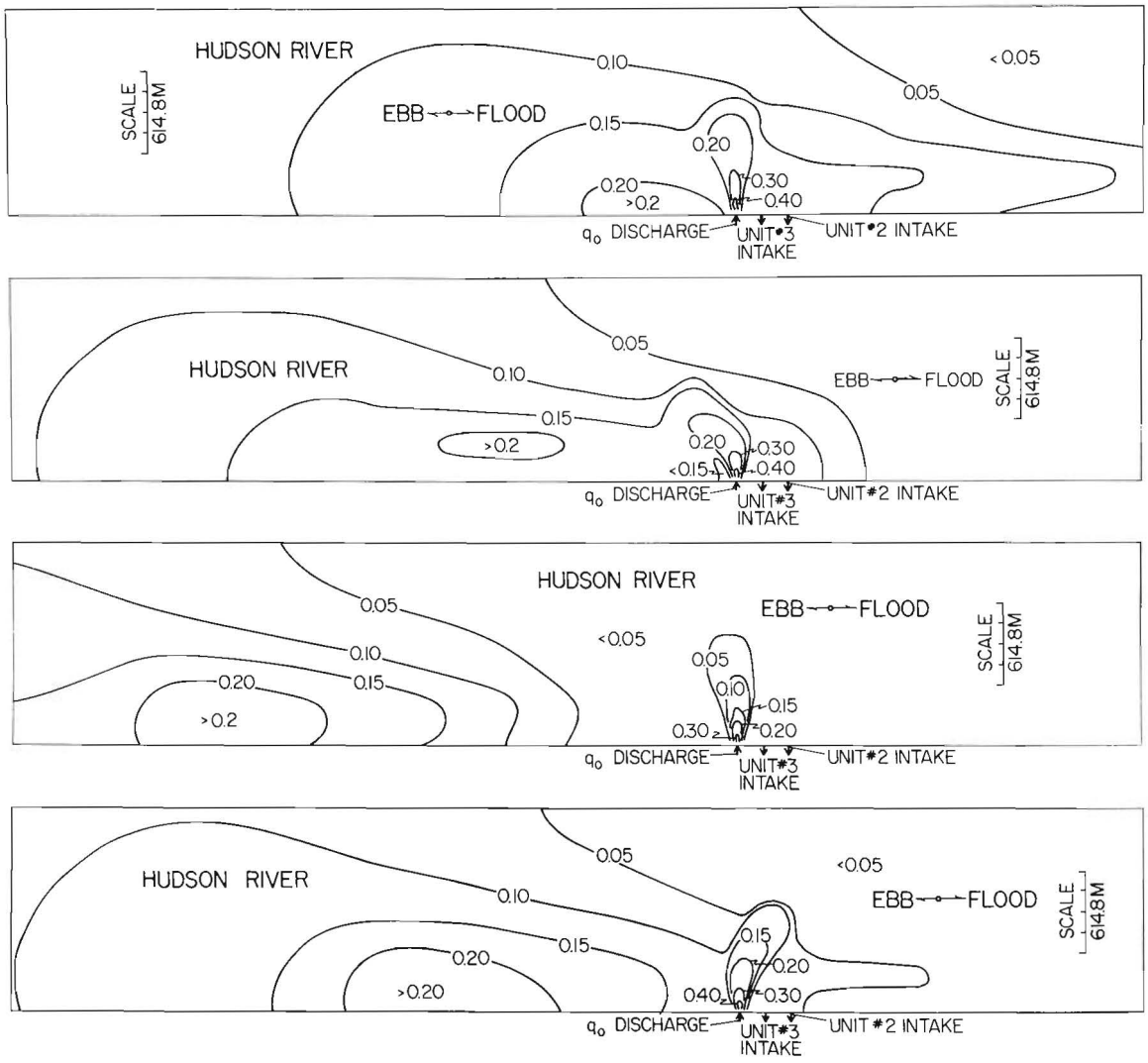

Figure 18. The surface excess temperature field predicted by the MSRC Complete Field Thermal Model for the cooling water discharge from Units 2 and 3 of the Indian Point generating facilities. Top (slack before ebb); second from top (maximum ebb); third from top (slack before flood); bottom (maximum flood).

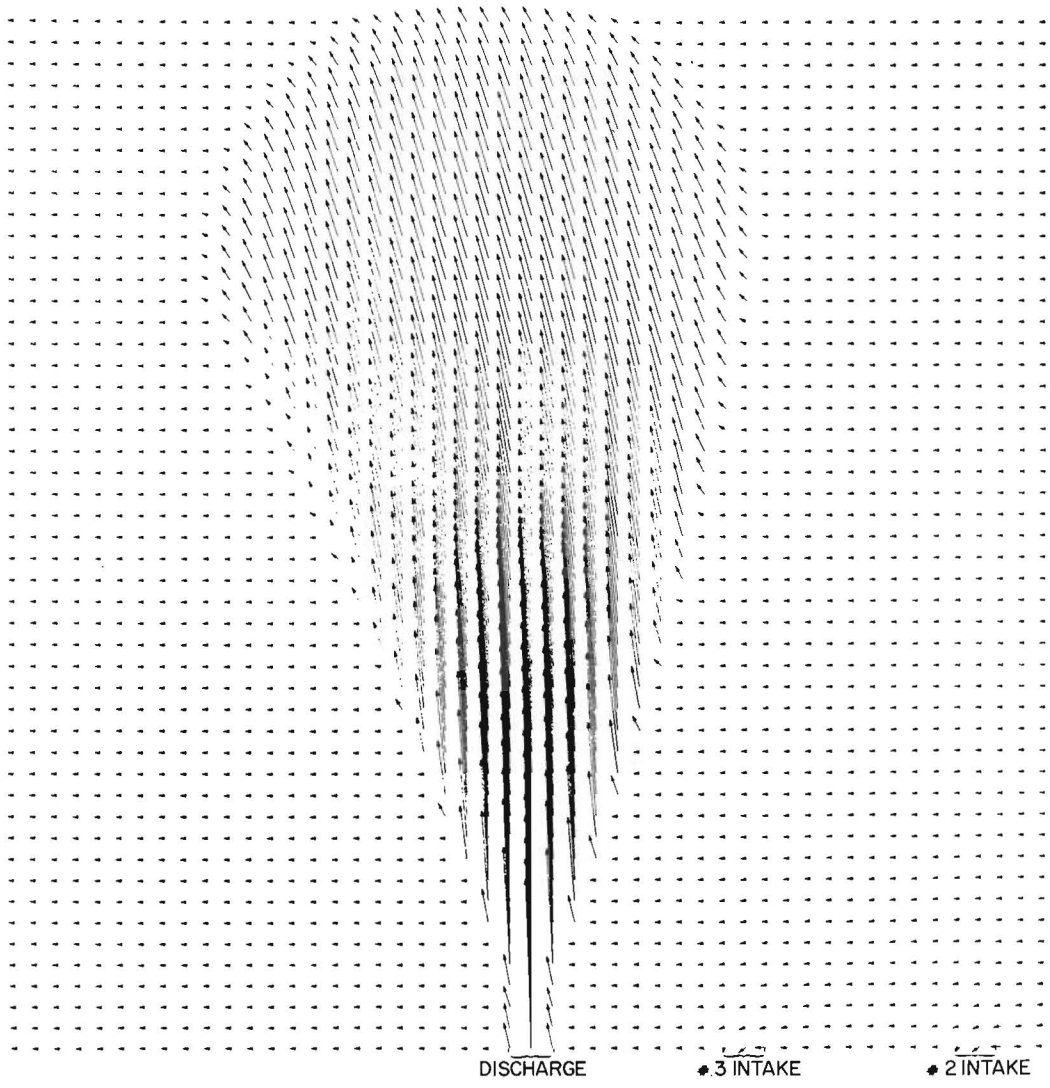

Figure 19a. The surface velocity field predicted by the MSRC Complete Field Thermal Model for the cooling water withdrawal and discharge from Units 2 and 3 of the Indian Point generating facilities at slack before ebb.

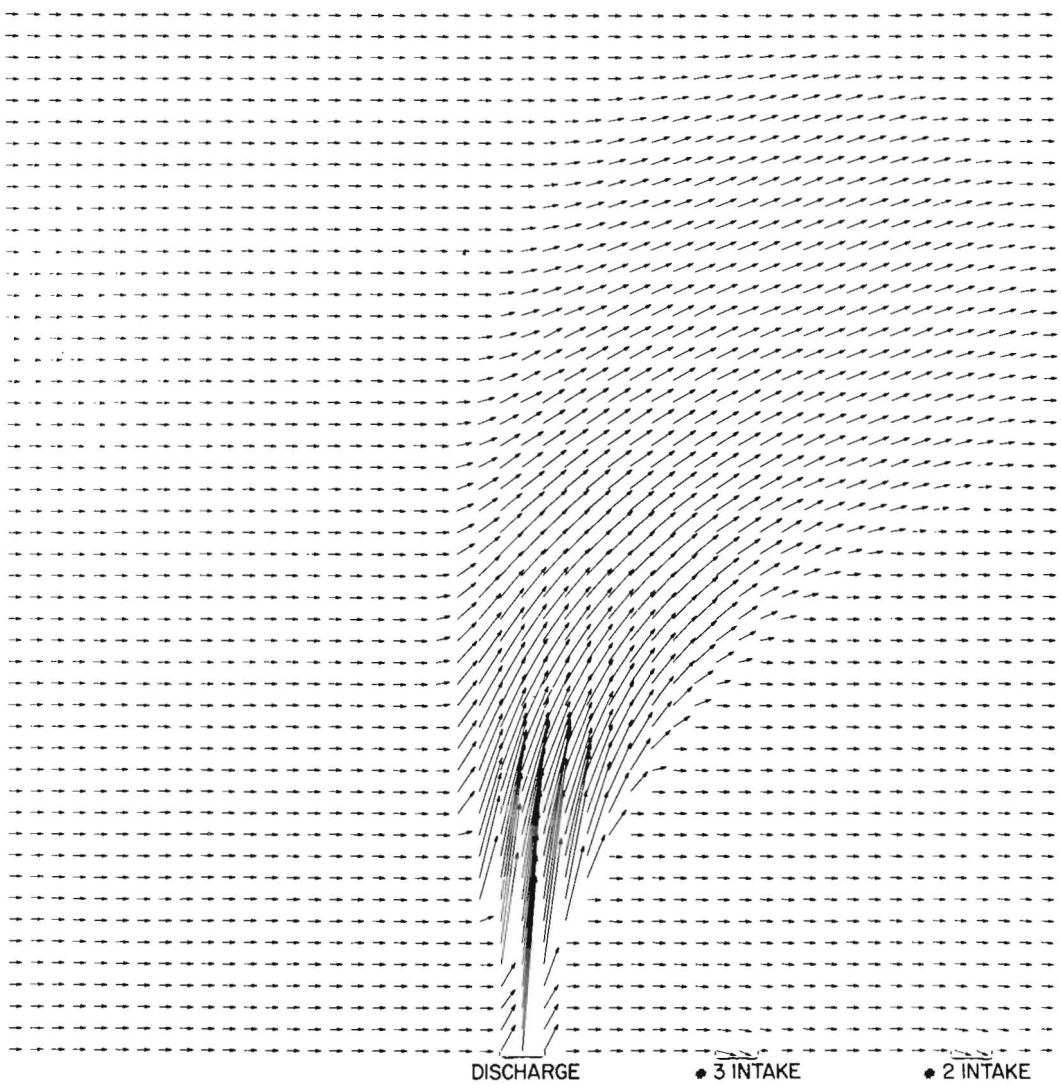

Figure 19b. The surface velocity field predicted by the MSRC Complete Field Thermal Model for the cooling water withdrawal and discharge from Units 2 and 3 of the Indian Point generating facilities at maximum flood.

results are shown in Figure 20. On Figure 20, θ^* has been rescaled to θ by multiplying by 9.18°C, the temperature rise across the condensers plus 8% recirculation (8.50 + 0.68). More precisely, one should account for recirculation in the model by allowing θ_0 and F_r to vary over the tidal cycle but simply rescaling θ^* is considered to be an acceptable approximation. The three organisms located in the lower left hand corner of the figure were drawn into the plant's intakes; as a result they will receive an additional dose of 5.508×10^3 °C-sec (9.18°C × 10 min × 60) if drawn into the Unit #2 intake and 2.754×10^3 °C-sec for Unit #3. In addition, they will be discharged with the cooling water after passing through the pumps and condensers and will, of course, experience an additional thermal dose. To estimate this dose, we released 20 organisms at intervals of 0.05 in t/T at the location of the discharge and calculated the resulting doses as before. The maximum excess temperature each experienced was obviously 9.18°C (θ_0 + recirculation). The results are summarized in Table 1. Thus the maximum dose[1] received by any organism was 3.574×10^4 °C sec. The fact that only the 3 organisms closest to the nearshore were drawn into the intakes suggests that their zone of influence is limited to 20-30 m in the lateral direction.

---

[1] 4.587×10^2 prior to entrainment by the pumps, 5.508×10^3 in the plant, and 2.9773×10^4 after discharge for a total of 3.574×10^4 °C sec.

---

3. Assessing the Biological Response to the Predicted Thermal Plume Exposures at Indian Point

In this report we consider only the effects of thermal stresses--the effects of physical or chemical stresses are not included in our analysis.

Those organisms usually considered most sensitive to thermal stresses are the egg and larval stages of finfishes and shellfishes (Schubel and Marcy, 1978). Protection of these life history stages should ensure adequate protection of Representative Important Species (R.I.S.) of phytoplankton and zooplankton. Criteria for identification as a Representative Important Species are given in EPA (1973) and R.I.S. of finfish for the Hudson River near Indian Point are listed in Ecological Analysts, Inc. (1978). Of those listed, we have chosen to concentrate on striped bass *(Morone saxatilis)* as it is considered most important in the eyes of the public and is a species for which there is a sufficient body of data on fractional mortalities due to thermal stresses.

Ecological Analysts, Inc. has carried out extensive thermal resistance experiments on various life stages of striped bass, white perch and alewife at their Indian Point field laboratory; the results are reported in EA (1978). Tables B-1 through B-170 in Appendix B to that report lists their actual experimental results (exposure temperature, time of exposure, sample size, and number of dead organisms) according to species, life stage, acclimation temperature, and salinity. From these tables we constructed thermal resistance curves similar to Figure 1 for striped bass post yolk sac larvae for the 10, 50, and 90% mortality levels at five acclimation temperatures between 15.0 and 23.5°C. From these curves the thermal doses that would produce mortalities in 10% of the experimental organisms as a function of temperature (acclimation plus excess) were calculated by graphical integration of the 10% curve. The results are plotted on Figure 21. The solid curve applies to an acclimation temperature of 15°C, the dashed curve to 20°C, and the dash-dot-dash curve to 23°C. All were fitted by eye to the data points. The

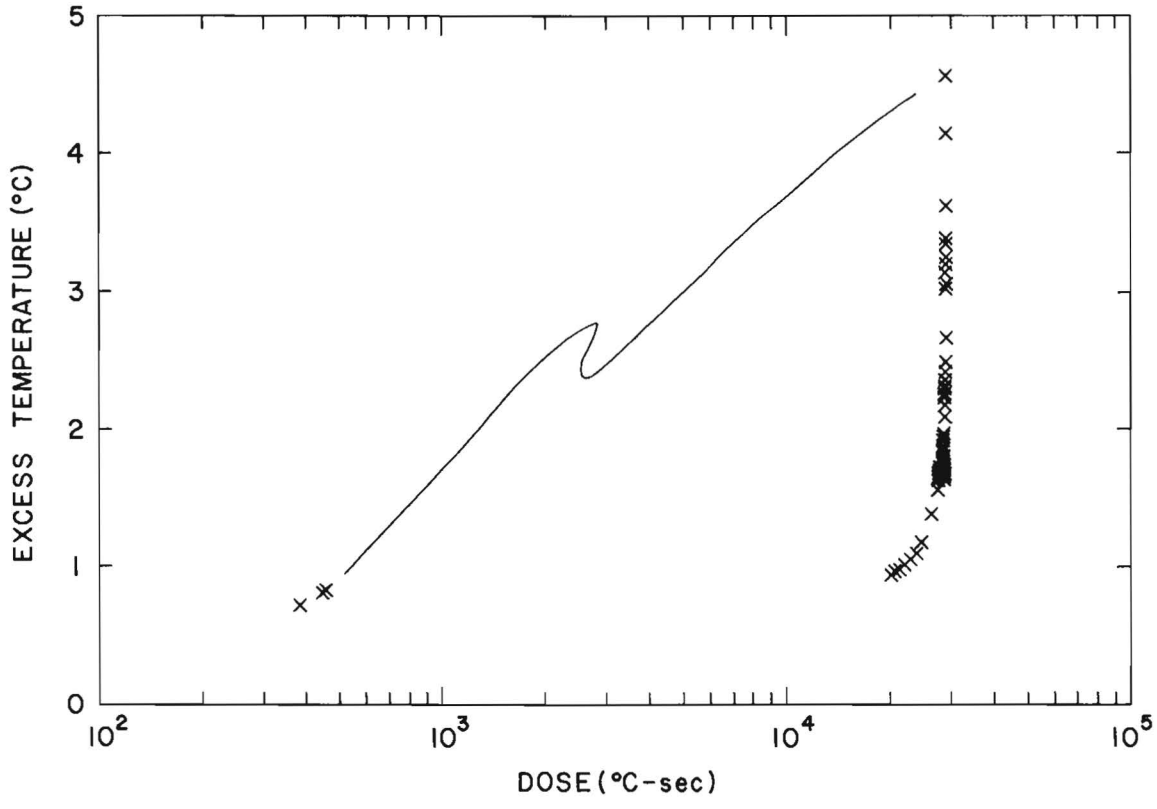

Figure 20. Thermal doses calculated with the MSRC Complete Field Thermal Model as a function of maximum excess temperature for 91 organisms initially distributed laterally across the Hudson River upstream from Indian Point. See text for details.

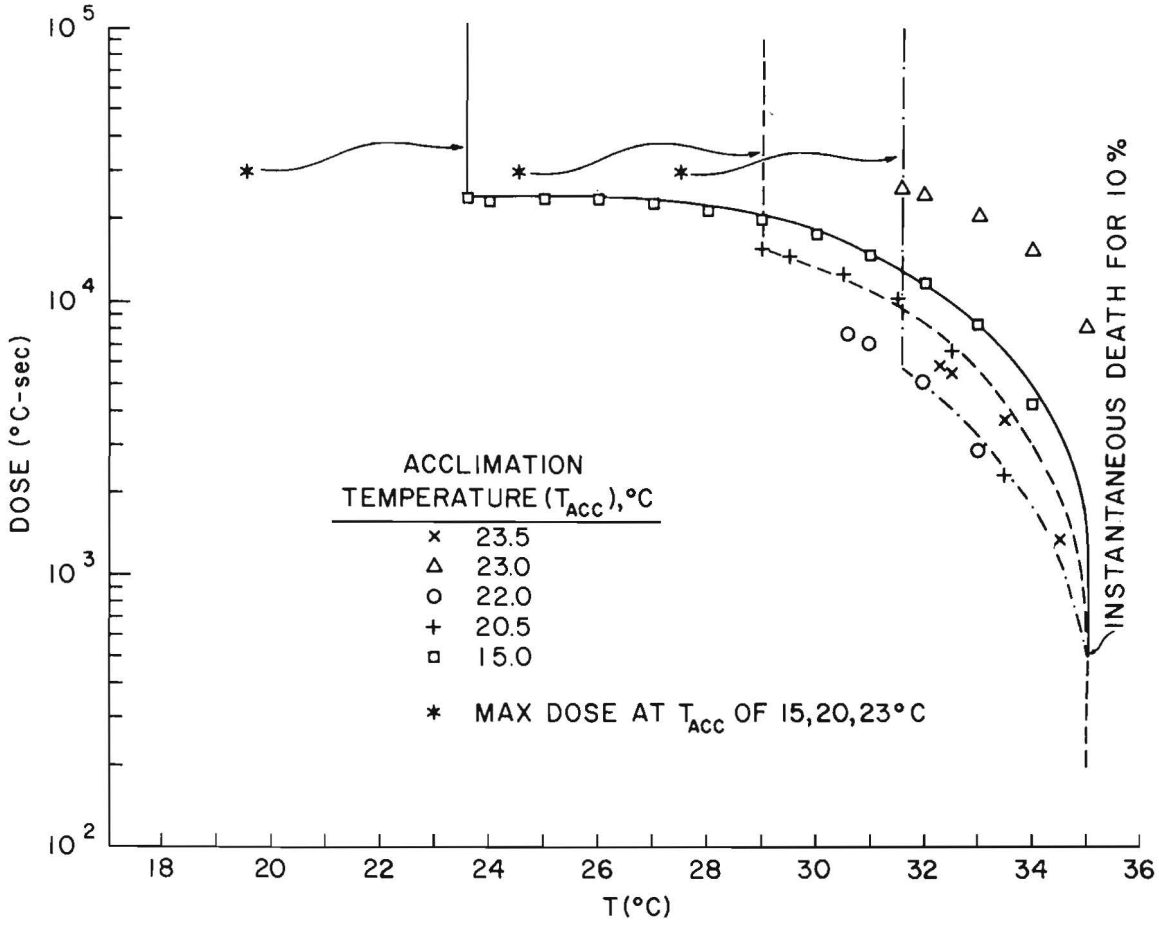

Figure 21. Comparison of the thermal doses predicted by the MSRC Complete Field Thermal Model for Indian Point with the Thermal Dose-Excess Temperature mortality curves (10%) for striped bass post yolk sac larvae acclimated to 15, 20, and 23°C. Thermal resistance laboratory data by Ecological Analysts (EA, 1978). The solid curve applies to an acclimation temperature of 15°C, the dashed curve to 20°C, and the dash-dot-dash curve to 23°C.

Table 1

Thermal Dose Received by Pump Entrained Organisms after Discharge in the Cooling Water at the Indian Point Generating Station

Organism #	Time Released, t/T	Dose, °C-sec	Maximum Excess Temperature
1	6.0	2.1291×10^4	9.18°C
2	6.05	2.1355×10^4	9.18°C
3	6.1	2.2566×10^4	9.18°C
4	6.15	2.7591×10^4	9.18°C
5	6.2	2.9716×10^4	9.18°C
6	6.25	2.7997×10^4	9.18°C
7	6.3	2.9108×10^4	9.18°C
8	6.35	2.7988×10^4	9.18°C
9	6.4	2.8658×10^4	9.18°C
10	6.45	2.8488×10^4	9.18°C
11	6.5	2.8296×10^4	9.18°C
12	6.55	2.7730×10^4	9.18°C
13	6.6	2.8068×10^4	9.18°C
14	6.65	2.8169×10^4	9.18°C
15	6.7	2.9773×10^4	9.18°C
16	6.75	2.8317×10^4	9.18°C
17	6.8	2.7198×10^4	9.18°C
18	6.85	2.5829×10^4	9.18°C
19	6.9	2.2846×10^4	9.18°C
20	6.95	2.2221×10^4	9.18°C

curves suggest that 10% of the experimental organisms will suffer instantaneous death at a temperature of 35°C regardless of acclimation temperature, and that organisms, acclimated to 15°C, 20°C, and 23°C can withstand continuous exposure to 23.6°C, 29.0°C, and 31.6°C, respectively (i.e., their incipient lethal temperatures). Also plotted on Figure 21 as * at the appropriate temperature (acclimation temperatures of 15, 20 and 23°C plus an excess of 4.6°C) is the maximum thermal dose experienced by any of the 88 plume entrained organisms. Since these points (*) lie to the left of the incipient lethal temperatures for post yolk sac larvae acclimated to 15, 20, or 23°C, it is clear that less than 10% of the striped bass post yolk sac larvae entrained in the heated plume from Units 2 and 3 will be killed. We reiterate, however, that this result applies only to those organisms that are entrained in the plume; organisms that are pump entrained are additionally subjected to physical stresses associated with velocity shear, abrasion, and pressure, and to chemical stresses if biocides are applied to prevent condenser tube fouling.

REFERENCES

Carter, H.H., E.W. Schiemer, R. Regier. 1973. The buoyant surface jet discharging normal to an ambient flow of various depths. Chesapeake Bay Institute, The Johns Hopkins University, Tech. Report #81, Ref. 73-7.

_____, and R. Regier. 1974. The three dimensional heated surface jet in a cross flow. Chesapeake Bay Institute, The Johns Hopkins University, Tech. Report #88, Ref. 74-8.

_____, J.R. Schubel, R.E. Wilson and P.M.J. Woodhead. 1977. A rationale for evaluating thermally induced biological effects due to once-through cooling systems. Marine Sciences Research Center, SUNY at Stony Brook, Special Report #7, Ref. 77-3.

Consolidated Edison Company of New York, Inc./Power Authority of the State of New York, July 1977. "Near-field Effects of Once-through cooling system operation on Hudson River Biota".

Consolidated Edison Company of New York Inc., August 1978. "Indian Point Nuclear Generating Station Thermal Survey Program, Routine Monthly Thermal Monitoring, June 1977 Survey, Report No. 3".

_____. Indian Point Generating Station, a 316(a) Demonstration, Appendix D, "Procedures and Analyses - Biological and Hydrothermal Studies".

Ecological Analysts, Inc. 1978. Hudson River Thermal Effects Studies for Representative Species, Final Report. Prepared for Central Hudson Gas & Electric Corp., Consolidated Edison Company of New York, Inc., Orange and Rockland Utilities, Inc.

EPA. 1973. Water Quality Criteria 1972, Ecological Research Series. EPA-R3-73-033, March 1973.

Gameson, A.L.H., J.W. Gibbs, and M.J. Barrett. 1959. A preliminary temperature survey of a heated river: Water and Water Engineering, January 1959; reprint No. 336 from Water Pollution Research Laboratory, Stevenage, Herts., England.

Hayashi, Taizo and Nobuo Shuto. 1967. Diffusion of warm water jets discharged horizontally at the water surface. Proc. 12th Congr. of Intl. Assoc. for Hydraulic Engrs. Vol. 4. Colorado State Univ., Fort Collins, Colorado.

Jen, Yuan, R.L. Wiegel, M. Asce, and I. Mobarek. 1966. Surface discharge of horizontal warm-water jet. J. Power Division. Proc. American Soc. Civil Engrs., Apr. 1966.

Milne-Thomson, L.M. 1960. Theoretical Hydrodynamics. The Macmillan Company, New York, 4th Edition.

Parkinson, F.E. and F. Goulet. 1976. Hydraulic Model Study of Hudson River Flows around cooling water Intakes. Lasalle Hydraulic Laboratory LTD Report LHL-682.

Pritchard, D.W. 1960. The application of existing oceanographic knowledge to the problem of radioactive waste disposal into the sea, *In* Disposal of radioactive wastes. Vol. 2. International Atomic Energy Agency, Vienna, pp. 229-248.

_____ and H.H. Carter. 1965. On the Prediction of the Distribution of Excess Temperature from a Heated Discharge in an Estuary. Chesapeake Bay Institute, The Johns Hopkins Univ., Tech. Rept #33, Ref. 65-1.

Prych, E.A. 1972. A warm weather effluent analysis as a buoyant surface jet. Swedish Meteorological and Hydrological Institute, Series Hyroli, No. 21.

Schubel, J.R. and R.C. Marcy, Jr. (eds). 1977. Power Plant Entrainment: A Biological Assessment. Academic Press, N.Y.

Shirazi, M.A. and L.R. Davis. 1974. Workbook of Thermal Plume Prediction Vol. 2, Surface Discharge. Environmental Protection Tech. Series, EPA-R2-72-005b.

Stolzenbach, K.D. and D.R.F. Harleman. 1971. An analytical and experimental investigation of surface discharges of heated water. Ralph M. Parsons Lab. for Water Resources and Hydrodynamics, Dept. Civil Engr., M.I.T. Report No. 135.

Tamai, N., R.L. Wiegel, and G.F. Tornberg. 1969. Horizontal surface discharge of warm water jets. J. Power Division, Proc. American Soc. Civil Engrs., Oct. 69, PO 2.

Wilson, R.E. 1978. A note on diffusion from a continuous line source in a time varying flow. Submitted to Water Resources Research.